



LUND UNIVERSITY

Zircon U-Pb-Hf evidence for subduction related crustal growth and reworking of Archaean crust within the Palaeoproterozoic Birimian terrane, West African Craton, SE Ghana

Petersson, Andreas; Scherstén, Anders; Kemp, Anthony; Bara, Kristinsdóttir; Per, Kalvig; Solomon, Anum

Published in:
Precambrian Research

DOI:
[10.1016/j.precamres.2016.01.006](https://doi.org/10.1016/j.precamres.2016.01.006)

2016

[Link to publication](#)

Citation for published version (APA):

Petersson, A., Scherstén, A., Kemp, A., Bara, K., Per, K., & Solomon, A. (2016). Zircon U-Pb-Hf evidence for subduction related crustal growth and reworking of Archaean crust within the Palaeoproterozoic Birimian terrane, West African Craton, SE Ghana. *Precambrian Research*, 275, 286–309.
<https://doi.org/10.1016/j.precamres.2016.01.006>

Total number of authors:
6

General rights

Unless other specific re-use rights are stated the following general rights apply:
Copyright and moral rights for the publications made accessible in the public portal are retained by the authors and/or other copyright owners and it is a condition of accessing publications that users recognise and abide by the legal requirements associated with these rights.

- Users may download and print one copy of any publication from the public portal for the purpose of private study or research.
- You may not further distribute the material or use it for any profit-making activity or commercial gain
- You may freely distribute the URL identifying the publication in the public portal

Read more about Creative commons licenses: <https://creativecommons.org/licenses/>

Take down policy

If you believe that this document breaches copyright please contact us providing details, and we will remove access to the work immediately and investigate your claim.

LUND UNIVERSITY

PO Box 117
221 00 Lund
+46 46-222 00 00

Accepted Manuscript

Title: Zircon U-Pb-Hf evidence for subduction related crustal growth and reworking of Archaean crust within the Palaeoproterozoic Birimian terrane, West African Craton, SE Ghana

Author: A. Petersson A. Scherstén A.I.S. Kemp B. Kristinsdóttir P. Kalvig S. Anum



PII: S0301-9268(16)00015-2
DOI: <http://dx.doi.org/doi:10.1016/j.precamres.2016.01.006>
Reference: PRECAM 4425

To appear in: *Precambrian Research*

Received date: 3-8-2015
Revised date: 16-11-2015
Accepted date: 6-1-2016

Please cite this article as: Petersson, A., Scherstén, A., Kemp, A.I.S., Kristinsdóttir, B., Kalvig, P., Anum, S., Zircon U-Pb-Hf evidence for subduction related crustal growth and reworking of Archaean crust within the Palaeoproterozoic Birimian terrane, West African Craton, SE Ghana, *Precambrian Research* (2016), <http://dx.doi.org/10.1016/j.precamres.2016.01.006>

This is a PDF file of an unedited manuscript that has been accepted for publication. As a service to our customers we are providing this early version of the manuscript. The manuscript will undergo copyediting, typesetting, and review of the resulting proof before it is published in its final form. Please note that during the production process errors may be discovered which could affect the content, and all legal disclaimers that apply to the journal pertain.

Highlights

- Zircon U-Pb-Hf isotope data suggest mainly juvenile growth between 2.3–2.1 Ga
- Reworking of Archaean crust in southern Ghana is confined to between 2.141–2.126 Ga
- Combined isotope data suggest subduction related crustal growth
- Emplacement of 2.23 Ga granodiorite contradict suggested plume initiated subduction
- An evolutionary model is proposed

**Zircon U-Pb-Hf evidence for subduction related
crustal growth and reworking of Archaean crust
within the Palaeoproterozoic Birimian terrane,
West African Craton, SE Ghana**

A. PETERSSON^{*1}, A. SCHERSTÉN¹, A.I.S. KEMP²,

B. KRISTINSDÓTTIR¹, P. KALVIG³, S. ANUM⁴

¹ Department of Geology, Lund University, Sölvegatan 12, SE-223 62 Lund, Sweden

² School of Earth and Environment, The University of Western Australia, Crawley, Australia

³ Geological Survey of Denmark and Greenland, 1350-Copenhagen, Denmark

⁴ Geological Survey Department, P.O. Box 672, Koforidua, Eastern Region, Ghana

^{*}Corresponding author (e-mail: andreas.petersson@geol.lu.se; phone: +46 462229553; fax: +46 462224830)

Abstract

Zircon Lu-Hf isotopic data from granites of southern and northwestern Ghana have been used to investigate the contribution of reworked Archaean bedrock to the Birimian crust of Ghana, West African Craton. Zircon from seven localities in southern Ghana and one locality in western Ghana were analysed. Combined U-Pb and Lu-Hf isotope data suggest juvenile crustal addition between 2.3–2.1 Ga, with a short period of reworking of Archaean crust. Until now, evidence for reworking of Archaean basement during Birimian magmatism in Ghana has hinged on whole-rock Nd model-

ages of the Winneba pluton, and sparse inherited zircon grains from mainly northwestern Ghana. Our data suggest that reworking of Archaean crust is greater than previously inferred, but was limited to between ~2.14–2.13 Ga. This period of reworking of older crustal components was preceded and succeeded by juvenile crustal addition. Coupled isotopic data suggest an eastward, mainly retreating arc system with a shorter pulse of accretion between ~2.18–2.13 Ga and a rapid return to slab retreat during the growth of the Birimian terrane. The accretionary phase initiated melting of sub-continental lithospheric mantle and the overlying Archaean crust, generating magma with sub-chondritic Hf signatures. Subsequent slab retreat led to trench-ward movement of the magmatic activity and the mixture of juvenile and Archaean crust was replaced by uncontaminated juvenile magma. The 2.23 Ga age of the West Accra granodiorite (PK105) demonstrates the emplacement of felsic rocks during the Eoeburnean and pre-dates the suggested plume related rocks, contradicting suggested plume initiated subduction.

1. Introduction

The formation of the Birimian terranes in West Africa (Fig. 1a–c) occurs towards the end of a period sometimes assumed to be associated with global magmatic quiescence (Condie, 2009). Yet, the formation of the Birimian crust has been cited as an example of rapid crustal growth, as large volumes of juvenile continental material were emplaced during a short time-span (Abouchami et al., 1990). Crystallisation ages from the Birimian bedrock of Ghana range between ~2.31 and 2.06 Ga, with a predominance of ages between 2.21 and 2.06 Ga (e.g. Gasquet et al., 2003; de Kock et al., 2011). These rocks have largely juvenile Nd isotope signatures (Abouchami et al., 1990; Liégeois et al., 1991; Boher et al., 1992; Ama-Salah et al., 1996; Hirdes et al., 1996; Doumbia et al., 1998; Gasquet et al., 2003; Pawlig et al., 2006; Klein et al., 2008; Tapsoba et al., 2013) with the exception of the Winneba pluton from southeastern Ghana, which has a $\epsilon\text{Nd}_{(2.173 \text{ Ga})} = -5.3$ and a depleted

59 mantle model age of ~ 2.6 Ga, indicating the involvement of Archaean crust (Taylor et al., 1990;
 60 Leube et al., 1990). Based on trace element geochemistry of mafic metavolcanic rocks, it has been
 61 proposed (Abouchami et al., 1990) that the Birimian crust formed rapidly and in response to mantle
 62 plume activity. Although alternative views such as arc accretion and convergent magmatism have
 63 been proposed (e.g. Sylvester and Attoh 1992; Feybesse and Milési 1994; Ama-Salah et al. 1996;
 64 Pouclet et al. 2006; Baratoux et al. 2011; de Kock et al. 2012), the Birimian terranes are still widely
 65 promoted as a prime example of mantle plume-related crust formation (c.f. Arndt, 2013).
 66 Feybesse et al. (2006) propose that the onset of continental crust growth within the Birimian terrane
 67 started at the end of the Eoeburnean (c. 2.35–2.15 Ga) phase, with the intrusion of abundant
 68 monzogranites between 2.16–2.15 Ga. Reworked Palaeoproterozoic to Archaean crust within the
 69 Birimian terrane is, apart from the Winneba pluton in southeastern Ghana (i.e. near the SE margin
 70 of currently exposed Birimian crust), only known through the presence of 2.26–2.88 Ga xenocrystic
 71 and commonly discordant zircon from rocks in the Bolé-Navrongo belt in northwestern Ghana e.g.
 72 the Gondo orthogneiss and the Ifantayire granite gneiss (Thomas et al., 2009; Siegfried et al., 2009;
 73 de Kock et al., 2011, Fig. 1c). Available geochronological data for the Birimian terrane, whole rock
 74 Lu-Hf and Sm-Nd isochrons for basalts (Blichert-Toft et al., 1999) and zircon U-Pb of granites
 75 (Hirdes et al., 1996) are coeval within error, i.e. they formed at 2.15 ± 0.05 Ga. Following a similar
 76 approach as Næraa et al. (2012), we explore coupled shifts in zircon U-Pb–Lu-Hf isotopes to
 77 explore crustal growth and reworking of older crust within an accretionary orogen. Detrital zircon
 78 $\delta^{18}\text{O}$ from five rivers draining Birimian bedrock in Ghana yield a weighted mean of 6.7 ± 0.2
 79 (MSWD = 5; Kristinsdóttir, 2013), which might indicate a significant reworked supracrustal
 80 component (c.f. Dhuime et al., 2012). Such an inference is in stark contrast with current models for
 81 the Birimian continental crust growth, which imply that the entire mass of juvenile crust formed
 82 around 2.15 Ga with the exception of the $2.173 \pm 0.107/-0.115$ Ga Winneba pluton (Taylor et al.,
 83 1988; Leube et al., 1990; Taylor et al., 1992).

As the median Birimian mantle composition as defined by Blichert-Toft et al. (1999) virtually coincides with the new crust curve presented by Dhuime et al. (2011) but is markedly lower than e.g. coeval depleted mantle values proposed by Griffin et al. (2000), the new crust curve of Dhuime et al. (2011), inferred from modern island arc basalts, is used as the depleted mantle reference in further discussion.

The samples in this study are mainly from the southernmost part of Ghana with the exception of the samples from the Sewfi belt granitoid (ASGH022A/C), which are from the Vinson quarry in the mid- to northwestern part of Ghana (Fig. 1). These rocks were sampled with the aim to further investigate the presence of reworked Archaean components within the Birimian terrane.

2. Geological settings

2.1. The southern West African Craton

The Reguibat Shield in the North and the (Leo-) Man Shield in the South make up the West African Craton in NW Africa (Fig. 1a). These Shields are separated by the Neoproterozoic–Palaeozoic Taoudeni basin. Archaean rocks are exposed in the western part of both shields and Palaeoproterozoic rocks of the Baoulé Mossi domain are abundant in the eastern part of the Man Shield (Fig. 1a and 1b). The Baoulé Mossi domain is juxtaposed with the Man Shield and formed along a ~2.1 Ga active accretionary margin during the Birimian event (Sylvester and Attoh, 1992; Feybesse and Milési, 1994; Vidal and Alric, 1994; Ama-Salah et al., 1996; Hirdes and Davies, 2002; Pouclet et al., 2006; Baratoux et al., 2011; de Kock et al., 2012), however, alternative interpretations including formation of continental crust at the margins of an oceanic plateau have been suggested (Abouchami et al., 1990; Boher et al., 1992). The Man Shield and the Baoulé Mossi domain are separated by the Sassandra fault (Abouchami et al., 1990; Attoh and Ekwueme, 1997; Fig. 1b). TTG gneisses > 3.0 Ga make up the oldest component in the Man Shield and are overlain by greenstone belts and in turn intruded by 2.97–2.78 Ga granites (Attoh and Ekwueme, 1997). On

the basis of lithological and age correlation, it has been suggested that the South American São Luis Craton and the Man Shield were united during the emplacement of the Birimian bedrock (e.g. Feybesse et al., 2006).

2.2. Birimian bedrock of the West African Craton

Birimian rocks of the Baoulé Mossi domain consists of 2.25–1.98 Ga volcanic belts, granitic gneisses and sedimentary basins, of which all have been affected by greenschist to amphibolite facies metamorphism (Milési et al., 1989; Boher et al., 1992; Ama-Salah et al., 1996; Hirdes et al., 1996; Peucat et al., 2005; Feybesse et al., 2006; de Kock et al., 2009; Baratoux et al., 2011). Volcanic belts and sedimentary basins trend NE-SW and make up the majority of the Palaeoproterozoic basement of Ghana (Fig. 1c; Leube et al., 1990; Hirdes et al., 1996). The volcanic belts are dominated by tholeiitic basalts at the base and calc-alkaline andesites, dacites and rhyolites in the upper sections (e.g. Boher et al. 1992; Sylvester and Atttoh, 1992). The metasedimentary basins are isoclinally folded and consist of volcanoclastic rocks, greywacke, argillitic rocks and chemical sedimentary rocks (Leube et al., 1990). There are four main suites of granite; Winneba, Cape Coast, Dixcove and Bongo. The rocks within the Winneba suite are restricted to a small area near the town of Winneba in southeastern Ghana and occur as granite to granodiorite. These are the only intrusions where Archaean Sm-Nd model ages hint at the involvement of reworked ancient crust (Leube et al., 1990; Taylor et al., 1988; 1992; Fig. 1c). The Cape Coast suite predominantly intrudes the metasedimentary basins and form larger plutons of peraluminous biotite-granodiorites (Leube et al., 1990). Dixcove suite rocks mainly intrude volcanic belts and form smaller plutons of metaluminous hornblende bearing granitic rocks and the younger Bongo type are potassium-rich granitic rocks that are found in northern Ghana and intrude the Tarkwaian sediments (Leube et al., 1990). Granodiorites and tonalities dominate these intrusions and granite (*sensu stricto*) only account for a minor part (Eisenlohr and Hirdes, 1992). The relative amount of granitic rocks within the volcanic belts in Ghana increase towards the northwest, which

has been interpreted as a function of erosional level, such that northwestern Ghana represents the deepest crustal sections exposed in the region (Taylor et al., 1992). The events that formed the basin and belt structure and subsequent geotectonic evolution is termed the Eburnean and prior events are termed the Eoeburnean (de Kock et al., 2011).

2.3. Growth of Birimian crust in Ghana

The majority of the Birimian terrane within the Baoulé Mossi domain consists of rocks that were emplaced around 2.2–2.1 Ga (Abouchami et al., 1990; Boher et al., 1992; Ama-Salah et al., 1996; Doumbia et al., 1998; Gasquet et al., 2003; Pawlig et al., 2006; Klein et al., 2008; Tapsoba et al., 2013) and with depleted mantle Nd model ages within 300 Myr. of their crystallisation ages (Boher et al. 1992) using the depleted mantle reference of Ben Othman et al. (1984). Using coupled Sm-Nd and Lu-Hf isotopes, the isotopic composition of the Birimian depleted mantle was determined to $\epsilon\text{Hf}_{(2.150\text{ Ga})} \approx 6 \pm 2$ and $\epsilon\text{Nd}_{(2.150\text{ Ga})} \approx 3 \pm 1$ (Blichert-Toft et al., 1999). The only known exception with the West African Craton that deviates significantly from this isotopic signature is represented by granitic rocks found in southeastern Ghana, the Winneba pluton. As noted above, Sm-Nd isotopic data from this body indicate incorporation of crustal material from an Archaean source (Leube et al., 1990, Taylor et al. 1992).

Gasquet et al. (2003) recorded a 2.312 ± 0.02 Ga (MSWD=8.1 n=8) xenocrystic zircon in a 2.170 ± 0.019 Ga granite from the Dabakala area (Fig. 1b). These xenocrystic zircon have been suggested to represent an early phase of crustal growth in the Baoulé Mossi domain. Feybesse et al. (2006) proposed a geodynamic model where the initial magmatic and tectonic activity that formed the Birimian bedrock in Ghana started at ~ 2.35 Ga with deposition of, for example, banded iron formations, which was followed by extensive emplacement of mafic to ultramafic crustal segments between 2.25–2.17 Ga. Mafic magmatism was followed by monzogranites between 2.16–2.15 Ga, which marks the first growth of continental crust in the Birimian terrane (Feybesse et al., 2006).

Metamorphism reached upper greenschist- to amphibolite facies during the Eburnean orogeny between ~2.13–2.00 Ga (Leube et al., 1990; Eisenlohr and Hirdes, 1992; Hirdes and Davis, 1998; Feybesse et al., 2006). Magmatic rocks younger than 2.07 Ga are scarce in the entire Baoulé Mossi domain, indicating a magmatic quiescence after this period (Gueye et al. 2007; de Kock et al. 2011).

3. Samples

3.1. PK101 Amasaman biotite hornblende tonalite (N 05° 42.730'/W 00° 16.270')

This rock is a weakly foliated medium- to coarse-grained biotite hornblende tonalite to granodiorite that was sampled in the central Suhum basin. It is cut by discordant late leucosomes with diffuse contacts with the main rock. It is dominated by nearly equigranular quartz and plagioclase.

Antiperthite occurs in some samples. Biotite is usually fresh. Secondary epidote-group minerals and muscovite overgrow feldspar, and minor amounts of intergranular calcite fills pore spaces and fractures (Fig. 2). Zircon is most commonly observed within biotite but also within quartz and feldspar.

The zircon population is euhedral to subhedral and grains vary in size from 50–500µm along their c-axis (Fig. 3). Most grains are oscillatory zoned and BSE-bright, with a thin (<20µm) BSE-dark rim of metamorphic zircon.

3.2. PK102 Nsawam biotite hornblende granite (N 05° 48.660'/W 00° 20.985')

This rock was sampled in a quarry in the town of Nsawam about 60 km northeast of Winneba. It is a coarse grained biotite hornblende granite, with green pleochroic biotite intergrown with abundant hornblende. Euhedral titanite is abundant and defines a weak tectonic fabric with biotite and hornblende. Secondary fine-grained muscovite and epidote overgrows feldspar and medium grained epidote with minor calcite occur along fractures and grain boundaries.

The zircon grains are 100–300µm along their c-axis, euhedral and display distinct oscillatory zonation in BSE (Fig. 4). Thin rims of metamorphic zircon cut the primary zonation in many grains and some grains have a BSE dark metamict appearance along cracks.

3.3. PK103 Gomoa Fetteh hornblende biotite granite (N 05° 26.185'/W 00° 28.372')

This hornblende biotite granite was sampled in the Krokrobite Tuba quarry close to the coast about 20 km east-northeast of the town of Winneba. Biotite and hornblende are roughly equal in abundance, with a slight tendency for greater amounts of biotite. K-feldspar is more abundant than plagioclase. Perthite is common and myrmekite intergrowths occur. Epidote, sometimes euhedral, is predominantly found along grain boundaries between feldspars and hornblende although some feldspar clouding might be due to fine secondary epidote. Minor amounts of calcite are localised along fractures. The mafic minerals have a slight preferred tectonic orientation.

Zircon grains are subhedral to euhedral and between 50–150 µm along their c-axis (Fig. 5). In BSE, oscillatory zonation is visible in most grains, but grains with a higher abundance of cracks have a more metamict and patchy appearance. Most grains have a thin rim of BSE bright secondary zircon truncating the primary zonation.

3.4. PK105 West Accra biotite hornblende granodiorite (N 05° 37.320'/W 00° 19.803')

This sample is a weakly foliated biotite hornblende granodiorite from the Suhum basin. The rock is coarse grained with patchy occurrence of secondary epidote, muscovite and calcite, mostly along fractures. The feldspar is slightly cloudy due to secondary fine grained epidote or muscovite.

Although the rock lacks conspicuous deformation features, quartz has recrystallised into subgrains.

The zircon grains are 50–500µm along their c-axis and morphologically euhedral to subhedral (Fig. 6). The zircon core domains are sector- or oscillatory-zoned and many grains have a thin BSE-bright rim of secondary zircon discordantly cutting zonation in the core.

3.5. ASGH003A Cape coast two-mica granodiorite (N 05° 20.759'/W 00° 36.828')

The outcrop is located in southern Cape Coast basin and is heterogeneous. Lithologies vary from fine to coarse grained, but medium to coarse grained varieties dominate. Metasedimentary xenoliths have higher contents of mafic minerals, of which biotite dominates. The sample investigated here is a coarse grained muscovite biotite granodiorite. Euhedral muscovite occur in minor amount but the majority is found together with biotite and at grain boundaries. The muscovite is interpreted to be primary. Feldspars are variably altered to sericite and perthite is common. Muscovite sometimes occur as secondary minerals on feldspar. Myrmekite inter-growths occur in minor amounts. The zircon population is between 50–150µm along their c-axis and mostly with euhedral morphology, many with sharp pyramid terminations (Fig. 7). Zircon grains are microstructurally complex, with BSE-bright oscillatory zoned cores discordantly cut by BSE-darker oscillatory zoned rims. Many grains have a patchy, metamict appearance in association with cracks. In less cracked grains the zonation is weaker to almost non detectable.

3.6. ASGH007A Dixcove hornblende tonalite (N 04° 47.609'/W 01° 56.733')

This hornblende tonalite is intrusive into Birimian volcanic flows and volcanoclastic sedimentary rocks. Angular basalt fragments are common and usually <10 cm in size. Minor amounts of fresh pyrite occur. It is medium to coarse grained rock with recrystallised quartz that forms sub-grains. Feldspars are undeformed and commonly subhedral to euhedral, forming a slightly porphyritic texture. Most grains are strongly saussuritised and sericitised but lack any tectonic fabric. Epidote ranges from fine saussurite to larger grains (100–150µm), and occurs with chlorite and sometimes minor amounts of calcite. The majority of the zircon in this sample is euhedral with sharp pyramid terminations (Fig. 8). In BSE, a weak oscillatory zonation is visible in most grains. The zonation in many grains is more pronounced towards grain boundaries.

3.7. ASGH022A/C Sunyani basin mica granites (N 07° 28.842'/W 02° 11.016')

These rocks were sampled from the Vision quarry in the Sunyani basin. The rocks within the quarry are diverse, with biotite muscovite to pure muscovite granites that contain schistose metasedimentary xenoliths of varying size (up to tens of metres).

Sample 22A is a biotite muscovite granite, and is the main rock type at the locality. It has abundant primary muscovite and lesser amounts of biotite. Plagioclase is the dominant feldspar but microcline occurs in lesser amounts. Most feldspars are slightly altered, primarily into sericite. The rock is equigranular and recrystallised with many grain boundaries forming 120° triple junctions.

Sample 22C is a late muscovite granitic pegmatite. The main difference between the pegmatite and the two-mica main granite is the near lack of biotite in the former. The feldspar composition is very similar to the two-mica granite (sample 22A), but it is slightly less altered.

The zircon populations in these rocks are identical in terms of morphology and texture and will be described together. Zircon grains are 50–150µm along their c-axis with a subhedral to euhedral morphology. Texturally they vary from well-preserved BSE-bright oscillatory zoned zircon to metamict BSE-dark and patchy zoned zircon (Fig. 9 and 10). Many grains have a thin rim of metamorphic zircon almost always associated with metamict BSE-dark textures.

4. Analytical methods

Zircon separation was done at the Department of Geology, Lund University. Rock samples were crushed by hand on a steel plate and clean chips were pulverised using a Cr-steel swing mill. Heavy minerals were separated on a Wilfley table, and collected in petri dishes. Magnetic fractions were removed using a magnetic pen and zircons were then hand picked under a binocular microscope. Selected grains were mounted on double sided tape together with the zircon standard 91500 (Wiedenbeck et al., 2004) and cast in epoxy. The epoxy mount was polished to expose internal cross sections through the grains. Back-scattered electron imaging (BSE) was used to investigate internal growth patterns in the individual crystals, and to guide the analytical work.

4.1. Zircon U-Pb dating

Secondary ionisation mass spectrometry (SIMS) U-Th-Pb analyses were carried out using a large geometry Cameca IMS1280 instrument at the Swedish Museum of Natural History in Stockholm. Instrument set up follows that described by Whitehouse et al. (1999), Whitehouse and Kamber (2005) and references therein. An O_2^- primary beam with 23 kV incident energy (-13kV primary, +10 kV secondary) was used for sputtering. For this study, the primary beam was operated in aperture illumination (Köhler) mode yielding a ca. 15-20 μm spot. Pre-sputtering with a 25 μm raster for 120 seconds, centring of the secondary ion beam in the 3000 μm field aperture (FA), mass calibration optimisation, and optimisation of the secondary beam energy distribution were performed automatically for each run, FA and energy adjustment using the $^{90}\text{Zr}_2^{16}\text{O}^+$ species at nominal mass 196. Mass calibration of all peaks in the mono-collection sequence was performed at the start of each session; within run mass calibration optimisation scanned only those peaks that yield consistently high signals from the zircon matrix, namely $^{90}\text{Zr}_2^{16}\text{O}^+$, $^{94}\text{Zr}_2^{16}\text{O}^+$ (nominal mass 204), $^{177}\text{HfO}_2^+$ (nominal mass 209), $^{238}\text{U}^+$ and $^{238}\text{U}^{16}\text{O}_2^+$, with intermediate peaks adjusted by interpolation. A mass resolution ($M/\Delta M$) of c. 5400 was used to ensure adequate separation of Pb isotope peaks from nearby HfSi^+ species. Ion signals were detected using the axial ion-counting electron multiplier. All analyses were run in fully automated chain sequences.

Data reduction assumes a power law relationship between Pb^+/U^+ and UO_2^+/U^+ ratios with an empirically derived slope in order to calculate actual Pb/U ratios based on those in the 91500 standard. U concentrations and Th/U ratio are also referenced to the 91500 standard. Common Pb corrections are made only when ^{204}Pb counts statistically exceed average background and assume a $^{207}\text{Pb}/^{206}\text{Pb}$ ratio of 0.83 (equivalent to present day Stacey and Kramers (1975) model terrestrial Pb). Decay constants follow the recommendations of Steiger and Jäger (1977). All age calculations were done in Isoplot 3.70 (Ludwig, 2008) and results are presented in Table 1.

4.2. Zircon Lu-Hf—*isotope analyses*

Lu-Hf analyses were carried out at the Advanced Analytical Centre at James Cook University in Townsville, Australia using a GeoLas 193-nm ArF laser and a Thermo-Scientific Neptune multi collector ICP-MS. Back scattered electron (BSE) images from a scanning electron microscope (SEM), transmitted and reflected light images were used to determine the optimum location of the spot on each zircon. Where possible, the Lu-Hf spots overlapped pits from the U-Pb analyses and spot sizes with a diameter of 31–58 μm were used. The interpreted crystallisation age of the individual sample was used in all Hf-isotope calculations. This age was also assumed for all undated (Lu-Hf isotope-) analysed grains of similar BSE character.

Each analysis began with a 30 second electronic baseline followed by an ablation period of 60 seconds involving 60 integration cycles of one second each. A laser pulse repetition rate of 4 Hz was used and the laser energy was held at $\sim 6 \text{ J/cm}^2$ which equals an ablation rate of 0.06 μm per pulse for zircon. Helium carrier gas was used to transport the ablated particles from the sample chamber. It was combined with argon gas (flow rate $\sim 0.8 \text{ l/min}$) and nitrogen ($\sim 0.005 \text{ l/min}$) further downstream before entering the argon plasma.

Masses 171 (Yb), 173 (Yb), 175 (Lu), 176 (Hf+Lu+Yb), 177 (Hf), 178 (Hf), 179 (Hf) and 180 (Hf+W+Ta) were measured simultaneously by Faradays detectors. Isobaric interference of ^{176}Yb and ^{176}Lu on ^{176}Hf was calculated using the measured intensities of ^{171}Yb and ^{175}Lu along with known isotopic ratios of $^{176}\text{Yb}/^{171}\text{Yb} = 0.897145$ (Segal et al. 2003) and $^{176}\text{Lu}/^{175}\text{Lu} = 0.02655$ (Vervoort et al. 2004). Mass bias corrections were calculated using the exponential law. For calculations of βHf , measured intensities of ^{179}Hf and ^{177}Hf and a $^{179}\text{Hf}/^{177}\text{Hf}$ ratio of 0.7325 was used. βYb was calculated using measured intensities of ^{173}Yb and ^{171}Yb and a $^{176}\text{Yb}/^{171}\text{Yb}$ ratio of 1.130172 (Segal et al. 2003). Mass bias behaviour of Lu was assumed to be identical to Yb.

Three standards were used for quality control, FC-1, Mud tank zircon (Woodhead and Herget 2005), and synthetic zircon (Fisher et al. 2011) and yielded $^{176}\text{Hf}/^{177}\text{Hf}$ of 0.282189 ± 0.00004 (2SD,

n=34), $^{176}\text{Hf}/^{177}\text{Hf}$ of 0.282500 ± 0.00003 (2SD, n=55) and $^{176}\text{Hf}/^{177}\text{Hf}$ of 0.282134 ± 0.00003 (2SD, n=24) respectively. These ratios are well within the range of solution mode data (Woodhead and Hergt 2005; Fisher et al. 2011) of FC-1 = $^{176}\text{Hf}/^{177}\text{Hf}$ of 0.282184 ± 16 ; Mud tank = $^{176}\text{Hf}/^{177}\text{Hf}$ of 0.282507 ± 6 ; Fisher synthetic = 0.282135 ± 7 . In addition, the stable Hf isotope ratios, $^{178}\text{Hf}/^{177}\text{Hf}$ and $^{180}\text{Hf}/^{177}\text{Hf}$, were monitored since these should be constant within error throughout the measurements. Analysed $^{176}\text{Hf}/^{177}\text{Hf}$ ratios of the unknown zircon grains were normalized based on comparison between the mean of analysed $^{176}\text{Hf}/^{177}\text{Hf}$ ratios of Mud tank zircon and its reported $^{176}\text{Hf}/^{177}\text{Hf}$ ratio of 0.282507 determined by solution analysis (Woodhead and Hergt 2005). Calculations of ϵHf use $\lambda^{176}\text{Lu} = 1.867 \times 10^{-11} \text{yr}^{-1}$ (Scherer et al. 2001; Söderlund et al. 2004), $(^{176}\text{Lu}/^{177}\text{Hf})\text{CHUR} = 0.0336$ and $(^{176}\text{Hf}/^{177}\text{Hf})\text{CHUR} = 0.282785$ (Bouvier et al. 2008). Two stage model ages were calculated using new crust values of $^{176}\text{Hf}/^{177}\text{Hf} = 0.28315$ and $^{176}\text{Lu}/^{177}\text{Hf} = 0.03795$ (Dhuime et al. 2011) and by assuming a $^{176}\text{Lu}/^{177}\text{Hf}$ of 0.0093 for the crustal source. Results are presented in table 2. Secondary standard analyses are shown in supplementary figure A.1 and listed in supplementary table A.2.

5. Results

5.1. PK101 Amasaman biotite hornblende tonalite

Fourteen spots from oscillatory-zoned zircon cores were analysed. Two of these are concordant while remaining twelve spots define a discordia with intercepts at 2.126 ± 0.012 Ga and 0.500 ± 0.057 Ga respectively (MSWD=2.2; Fig. 11a). The upper intercept is interpreted to date the crystallisation age of this sample, while the lower intercept is in accordance with Pan-African Pb-loss in the response to the Dahomeyan orogen <10 km to the southeast. U and Th/U range between 267–628 ppm and 0.07–0.84 respectively. One analysis n3762-03 was discarded due to high common Pb ($^{206}\text{Pb}/^{204}\text{Pb}=124$) and associated large error.

Nine Hf isotope analyses (of which #10 was discarded due to the laser penetrating the grain) yield $^{176}\text{Lu}/^{177}\text{Hf} < 0.0008$, $^{176}\text{Yb}/^{177}\text{Hf} < 0.03$ and $^{176}\text{Hf}/^{177}\text{Hf}$ from 0.281338 to 0.281416. The corresponding $\varepsilon\text{Hf}_{(2.126 \text{ Ga})}$ values range between -4.2 and -1.3 (Fig. 11).

5.2. PK102 Nsawam biotite hornblende granite

In this sample, only oscillatory-zoned zircon core domains were analysed. A regression of all data points (n=16) yield a lower intercept of $0.523 \pm 0.096 \text{ Ga}$, which points to Pan-African Pb-loss, and an upper intercept of $2.174 \pm 0.006 \text{ Ga}$ (MSWD=2.5; Fig. 11b), which is interpreted as the igneous crystallisation age of this sample. U concentrations range between 150–545 (150–425 ppm for data points used for concordia calculation) and Th/U range between 0.30–0.59 (0.38–0.59 for data points used for concordia calculation).

Nineteen Hf isotope analyses from eighteen grains yield $^{176}\text{Lu}/^{177}\text{Hf} < 0.0023$, $^{176}\text{Yb}/^{177}\text{Hf} < 0.07$ and $^{176}\text{Hf}/^{177}\text{Hf}$ range from 0.281454 to 0.281590. $\varepsilon\text{Hf}_{(2.174 \text{ Ga})}$ ranges between +0.7 and +5.2 (Fig. 11).

5.3. PK103 Gomoa Fetteh hornblende biotite granite

Sixteen analyses of oscillatory zoned core domains were analysed. One slightly discordant spot (n3763-15) with a $^{207}\text{Pb}/^{206}\text{Pb}$ -date of $2.460 \pm 0.015 \text{ Ga}$ is of xenocrystic origin. Remaining spots define a discordia with intercepts at $2.139 \pm 0.005 \text{ Ga}$ and $0.431 \pm 0.110 \text{ Ga}$ (MSWD=1.5; Fig. 11). The $2.139 \pm 0.005 \text{ Ga}$ intercept is interpreted as the igneous crystallisation age of this sample. U concentrations range between 38–382 ppm and Th/U range between 0.31–1.35, with no correlation with discordance.

Fourteen Hf isotope analyses of magmatic domains (two were discarded) yield $^{176}\text{Lu}/^{177}\text{Hf} < 0.0016$ and $^{176}\text{Yb}/^{177}\text{Hf} < 0.05$ and $^{176}\text{Hf}/^{177}\text{Hf}$ range from 0.281340 to 0.281516. $\varepsilon\text{Hf}_{(2.139 \text{ Ga})}$ ranges between -3.8 and +1.7 (Fig. 11).

5.4. PK105 West Accra biotite hornblende granodiorite

Fifteen spots are discordant beyond the 2σ -level and might represent a combination of Pan-African and recent Pb-loss (Fig. 11). In order to avoid the Pan-African overprint, concordant data with ($^{206}\text{Pb}/^{204}\text{Pb} > 10\,000$) were used to calculate a weighted average $^{207}\text{Pb}/^{206}\text{Pb}$ -date, which yielded 2.229 ± 0.004 Ga (MSWD=0.7; $n=12/13$; Fig. 11). We interpret this date as the best estimate of the igneous crystallisation age. U concentrations range between 101–638 ppm with a negative correlation between U concentration and $^{207}\text{Pb}/^{206}\text{Pb}$ -date. All analyses used to calculate the concordia age have <250 ppm U. Th/U for all analyses range between 0.09–0.64. Twenty-eight Hf isotope analyses from 26 different grains yield $^{176}\text{Lu}/^{177}\text{Hf} < 3.1 \times 10^{-3}$ and $^{176}\text{Yb}/^{177}\text{Hf} < 0.08$ and $^{176}\text{Hf}/^{177}\text{Hf}$ range from 0.281499 to 0.281645. Corresponding $\epsilon\text{Hf}_{(2.229\text{ Ga})}$ values range between +2.0 and +6.3 (Fig. 11). Two analyses (-09, -10) were discarded, both due to short analysis time.

5.5. ASGH003A Cape coast two-mica granodiorite

Twenty-two analyses from different domains form a loosely defined discordia with intercepts at 2.097 ± 0.041 Ga and 0.408 ± 0.030 Ga respectively (MSWD=9.6). Three analyses are concordant, all from BSE bright oscillatory zoned domains, and yield a $^{207}\text{Pb}/^{206}\text{Pb}$ -date of 2.125 ± 0.018 Ga (MSWD=1.8; Fig. 11). This is interpreted as the igneous crystallisation age and is older than the 2.090–2.095 Ga age bracket given by 2.090 ± 0.002 Ga monazite and slightly discordant 2.095 ± 0.0034 Ga zircon, where Pan-African Pb-loss was not accounted for (Davies et al., 1994). U concentrations range between 579–5726 ppm (588–855 ppm for concordant data-points) and Th/U range between 0.00–0.10 (0.55–0.83 for concordant data-points). There is a negative correlation between U concentration and $^{207}\text{Pb}/^{206}\text{Pb}$ -dates.

Twenty-three Hf isotope analyses in 21 grains of which two were discarded due to the laser drilling thorough the grains (n3682-Hf-06, -13) and one (n3682-1b) due to heterogeneous $^{176}\text{Hf}/^{177}\text{Hf}$ signal, yield $^{176}\text{Lu}/^{177}\text{Hf} < 1.6 \times 10^{-3}$ and $^{176}\text{Yb}/^{177}\text{Hf} < 0.05$ and $^{176}\text{Hf}/^{177}\text{Hf}$ ranges from

0.281447 to 0.281620. The $\epsilon\text{Hf}_{(2.125\text{ Ga})}$ values range between -0.1 and +5.4 with a majority of the data (n=18) clustering between +2.1 and +4.3 (Fig. 11).

5.6. ASGH007A Dixcove hornblende-granite

Twelve analyses of oscillatory-zoned core domains yield data that are between 2.5–71.1% discordant beyond the 2σ -level. There is a clear trend with increased U concentration and discordance in domains with strong zonation. Discarding the three most discordant and U-rich analyses, all from strongly zoned domains, a weighted average $^{207}\text{Pb}/^{206}\text{Pb}$ -date of $2.173 \pm 0.012\text{ Ga}$ (MSWD=1.4, probability=0.2; Fig. 11) is obtained. Our date is in excellent agreement with the $2.172 \pm 0.002\text{ Ga}$ date obtained by Hirdes et al., (1992), and we interpret this as the igneous crystallisation age of the granite. U concentrations range between 71–1291 (71–118 ppm for concordant data points) and Th/U range between 0.03–0.51 (0.31–0.51 for concordant data points). Nine Hf isotope analyses yield $^{176}\text{Lu}/^{177}\text{Hf} < 0.8 \times 10^{-3}$ and $^{176}\text{Yb}/^{177}\text{Hf} < 0.03$ and $^{176}\text{Hf}/^{177}\text{Hf}$ range from 0.2814479 to 0.281573. $\epsilon\text{Hf}_{(2.173\text{ Ga})}$ values range between +1.3 and +5.2 (Fig. 11).

5.7. ASGH022A Sunyani basin two-mica granite

Eleven oscillatory zoned core domains were analysed, of which all but two are concordant within error. The data define a discordia with intercepts at $0.152 \pm 0.260\text{ Ga}$ and $2.093 \pm 0.002\text{ Ga}$ (MSWD = 0.9; Fig. 11) which is compatible with a recent Pb-loss model. The weighted average $^{207}\text{Pb}/^{206}\text{Pb}$ -date of all spots yield a $2.093 \pm 0.002\text{ Ga}$ (MSWD=0.9; n=11/11; Fig. 11), and is interpreted as the igneous crystallisation age of this sample. U concentrations and Th/U range between 101–1273 and 0.07–0.67 respectively.

Hf isotope analyses (n=9) yield $^{176}\text{Lu}/^{177}\text{Hf} < 0.3 \times 10^{-3}$ and $^{176}\text{Yb}/^{177}\text{Hf} < 0.01$ and $^{176}\text{Hf}/^{177}\text{Hf}$ range from 0.281551 to 0.281587. Corresponding $\epsilon\text{Hf}_{(2.093\text{ Ga})}$ values range between +3.4 and +4.9 (Fig. 11).

5.8. ASGH022C Sunyani basin pegmatite

Seven analyses of BSE-bright oscillatory zoned core domains yield a discordia with only one intercept at 2.082 ± 0.010 Ga (MSWD=1.1; Fig. 11). The weighted average $^{207}\text{Pb}/^{206}\text{Pb}$ -date of all spots yield a 2.092 ± 0.004 Ga (MSWD=1.2; $n=7/7$; Fig. 11), which is interpreted as the crystallisation age of this sample. U concentrations and Th/U range between 239–447 and 0.25–0.43 respectively.

Seven Hf isotope analyses yield $^{176}\text{Lu}/^{177}\text{Hf} < 0.3 \times 10^{-3}$ and $^{176}\text{Yb}/^{177}\text{Hf} < 0.01$ and $^{176}\text{Hf}/^{177}\text{Hf}$ range from 0.281547 to 0.281606. The $\epsilon\text{Hf}_{(2.092 \text{ Ga})}$ values range between +3.2 and +5.5 (Fig. 11).

6. Discussion

6.1. Juvenile granitic crust within the Birimian terrane

At the present day, the West African Craton is cut by, and juxtaposed with, juvenile Pan-African (Dahomeyan) crust in the southeast (e.g. Affaton et al., 1991). The paleo-extent of this Craton is unknown. However, as documented here, granite ages extend to >2.2 Ga towards its eastern margin, which are among the oldest within the Eburnean orogeny, and predate most mafic volcanic suites elsewhere in the Birimian terrane. The mafic volcanism has been ascribed to the arrival of a mantle plume (Abouchami et al., 1989) as well as subduction related volcanism (Sylvester and Attah, 1992). Irrespective of tectonic model, the mafic magmatism is considered to represent juvenile crust generation between 2.15 to 2.2 Ga. To this end, it is notable that the >2.2 Ga granite magmatism that is documented here through sample PK105 has $\epsilon\text{Hf}_{(2.229 \text{ Ga})} = +2.0$ – $+6.3$, in line with estimates for the sub-lithospheric Birimian mantle from mafic volcanic rocks (Blichert-Toft et al., 1999), and implying derivation from juvenile crust.

More recently, it has been argued that Eoeburnean (c. 2.35–2.15 Ga) rocks have equivalents in various parts of the West African Craton and in the Brazilian São Luis Craton (deKock et al., 2011). These rocks are thought to correspond to a long-lasting period of juvenile crust formation (deKock

et al., 2011). This is seen in the Eoeburnean Hf isotopic record where all combined zircon U-Pb-Hf data yield juvenile supra-chondritic ϵ_{Hf} values (Fig. 12). Eoeburnean rocks crop out in an area extending from southwestern Ivory Coast and Liberia to Burkina Faso and Ghana, with a few occurrences of Eoeburnean rocks reported from eastern Guinea (Lahondère et al. 2002) and southern Mali (McFarlane et al., 2011). Based on inherited 2.312 ± 0.02 Ga zircon and literature Sm-Nd model ages, Gasquet et al. (2003) proposed an early phase of crustal growth within the Baoulé Mossi around 2.3 Ga. Early onset of the Birimian event has also been argued for by Feybesse et al. (2006) based on ~ 2.35 Ga rocks within the Brazilian Boromea belt. This early stage of evolved magmatic activity in the Birimian event contradicts the global 2.45–2.20 Ga magmatic quiescence proposed by e.g. Condie et al. (2009) but is in line with the more recent views of Partin et al. (2014) who argue for uninterrupted Palaeoproterozoic plate tectonics. Feybesse et al. (2006) suggests that juvenile crust formed during the Eoeburnean phase was thickened through accretion between 2.16–2.15 Ga, coeval with the emplacement of large volumes of monzonitic plutonic complexes found both in southern Ghana and in the São Luis Craton. Between 2.15–2.10 Ga several basins (e.g. Sunyani, Kumasi-Afema and Comoé basins) formed during an extensional tectonic regime (Feybesse et al., 2006). The initial part of this extensional phase is coeval with a narrow span in crystallisation ages between 2.14–2.13 Ga that drop to sub-chondritic ϵ_{Hf} values (Fig. 12). A similar drop is observed in detrital zircon data (Kristinsdóttir, 2013). This suggests that the reworking of Archaean crust within the Birimian terrane is limited to this time-slice, and that it was preceded and succeeded by juvenile continental crust formation with minimal or no contamination by older crust. This is in line with the detrital zircon record, which is dominated by 2.15–2.06 Ga crystallisation ages and juvenile isotopic signatures (Kristinsdóttir, 2013; Izuka et al., 2013). Further work to explore the amount of reworked crust elsewhere in the West African Craton is, however, required.

6.2. Reworking of Archaean material within the Birimian terrane

Our new zircon Lu-Hf data for c. 2.14–2.13 Ga granites from the Suhum basin display predominantly negative ϵ_{Hf} , indicating significant involvement of older, tentatively Archaean, reworked crust (Fig. 12). This result corroborates whole rock Nd isotope data from the Winneba pluton in the Kibi-Winneba belt that yield a model age of c. 2.6 Ga (Leube et al., 1990; Taylor et al., 1992). Our new data extends the area where an Archaean signature is identified to include the Suhum basin southeast of the Kibi-Winneba belt (Fig. 12). Recalculating the Nd isotope data of Taylor et al. (1990) to ϵ_{Hf} using equation: $\epsilon_{\text{Hf}} = 1.55 \times \epsilon_{\text{Nd}} + 1.21$, as suggested by Vervoort et al., (2011) the Winneba pluton yields $\epsilon_{\text{Hf}} = -7.2$ (Fig. 12). This is even lower than the zircon data obtained here, but independent Hf isotope data or further work is required to test the validity of this correlation.

We calculate two stage model ages using the measured $^{176}\text{Lu}/^{177}\text{Hf}$ and the age of the zircon for the first stage, and an assumed $^{176}\text{Lu}/^{177}\text{Hf}$ value of 0.0093 and the new crust curve of Dhuime et al. (2011) as a depleted mantle reference for the second stage.

Considering the $\epsilon_{\text{Hf}}(2.150 \text{ Ga}) \approx 6 \pm 2$ estimate of the Birimian mantle provided by Blichert-Toft et al. (1999), a moderately depleted mantle evolution as suggested by Dhuime et al. (2011) or Iizuka et al. (2013) seems justified. The most enriched samples (PK101 and PK103) yield 2.4–2.7 Ga model ages (Table. 2). In addition to Lu-Hf based model ages, a xenocrystic zircon with a $^{207}\text{Pb}/^{206}\text{Pb}$ -date of 2.460 ± 0.015 Ga was found in sample PK103 (Fig. 1b, Table 1), providing additional evidence for the reworking of older crust. Irrespective of mantle model, a majority of the analysed grains from southern Ghana require reworking of an ancient component to explain their Hf isotope ratios. This suggests a more substantial contribution of reworked Archaean crust to the southern parts of the Birimian terrane in Ghana than previously known.

Detrital zircon grains from the Cadomian Orogen in central west Europe include a 1.8–2.2 Ga component that is interpreted to have derived from the West African Craton (Linnemann et al., 2014). The model ages of this population imply reworking of a 2.5–3.4 Ga basement, using a MORB-mantle depletion model. Furthermore, detrital zircon from the Anti-Atlas belt in southern

Morocco have an Archaean component with Hf model ages varying between 2.3 and 3.3 Ga (Abati et al., 2012). The origin of these grains is unknown, but the agreement between the Anti-Atlas zircon model ages and the least radiogenic data from southern Ghana opens for the possibility of a Birimian source to these zircon grains. However, the inference about the antiquity of the West African Craton by Linnemann et al. (2014) is only partly conceivable when compared with our results, where significant reworking of ancient crust appears to be limited to a period between 2.14 to 2.13 Ga. Their conclusion is in stark contrast with the generally juvenile nature of Birimian rocks, which is supported by our data as well as having been noted in previous studies (e.g. Abouchami et al., 1990; Liégeois et al., 1991; Boher et al., 1992; Ama-Salah et al., 1996; Hirdes et al., 1996; Doumbia et al., 1998; Gasquet et al., 2003; Pawlig et al., 2006; Klein et al., 2008; Tapsoba et al., 2013). Further study is required to establish the degree as well as the spatial and temporal distribution of reworking of Archaean crust across the West African Craton.

6.3. On the scarcity of xenocrystic zircon

The small number of pre-Eburnean xenocrystic zircon found in this study ($n = 1$) and within the Birimian terrane of the West African Craton as a whole ($n \approx 40$; c.f. De Kock et al., 2011) is curious given our Hf isotope evidence for reworking of ancient crust (Fig. 12). This might be explained by a zircon poor or absent protolith, reflect biased sampling or physiochemical properties of magmas that caused resorption of inherited zircon.

The phenomenon with a few zircon xenocrysts in rocks that have enriched isotope signatures, indicating reworked older crust, is not unique to the Birimian terrane. Similar observations are made both in regional and global datasets. For example, Eoarchaeon to Neoarchaeon basement rocks in southern West Greenland with variably enriched zircon Hf isotope signatures that were interpreted to have crystallised from reworked older continental crust lack or have few xenocrystic zircon (Hiess et al., 2011; Næraa et al., 2012; 2014). In the case of the 2.55 Ga Qorqû granite in southern

West Greenland, Næraa et al., (2014) argued that the source rock was Eoarchaeon mafic crust, which likely would supply few xenocrystic zircon grains to the magma.

Palaeo- to Mesoproterozoic intrusions in southern Fennoscandia that intrude and rework metasedimentary basins have few xenocrystic zircon grains (Petersson et al., 2015a; 2015b). In these two studies, the scarcity of xenocrystic zircon might in part be due to sampling bias as euhedral simple magmatic zircon was targeted (Petersson et al., 2015b), or the alkaline nature of some magmas might have dissolved zircon to a higher extent (Petersson et al., 2015a).

In contrast to these studies, a large number of xenocrystic zircon was retrieved from rocks crystallised from initially zircon-undersaturated magmas within the Phanerozoic Lachland Orogen (Kemp et al., 2005).

On a global scale, there is a similar enigmatic discrepancy between the small amount of pre-3.0 Ga zircon (ca. 10%) and the large inferred mass fraction of continental crust (50 – 70% of the present mass; Belousova et al., 2010; Dhuime et al., 2012).

To what extent the scarcity of xenocrystic zircon within the Birimian terrane represent sampling bias, source characteristics or zircon dissolution due to physiochemical magma properties remains unclear.

6.4. Birimian isotopic signatures in a tectonic context

The Birimian crust is a commonly cited example (e.g. Arndt, 2013) of plume-related crustal growth, where the mafic volcanism has been proposed to represent the first stage of the crustal evolution (Abouchami et al. 1990; Vidal et al. 1996; Doumbia et al. 1998; Lompo 2009, 2010; Vidal et al. 2009). Boher et al. (1992) propose a model where the Birimian crust initially formed a plume-related oceanic plateau around which subduction zones subsequently reworked the oceanic plateau before it was accreted to the Archaean nucleus of the Man Shield. The main arguments for this interpretation include – the common occurrence of pillow lavas and the absence of rocks with

546 affinities of the continental crust, the juvenile isotopic character of the Birimian terrane and the
 547 geochemical signatures of the Birimian mafic supracrustal rocks.
 548 In contrast, other workers have argued for a subduction setting for basaltic and andesitic rocks
 549 within the Birimian crust (e.g. Sylvester and Attoh, 1992; Evans et al., 1996; Ama Salah et al.,
 550 1996; Baratoux et al, 2011). The juvenile character of the Birimian terrane is the single unifying
 551 interpretation, which is based on the scarcity of xenocrystic zircon and Sr, Nd and Hf isotopic
 552 compositions that indicate purely juvenile crustal growth.
 553 If a mantle plume model is based on characteristics of comparatively well-established Phanerozoic
 554 analogs such as the Deccan–Reunion or the Parana-Etendeka–Tristan da Cunha, the main eruptive
 555 stage of flood basalt volcanism should last for c. 1 Myr (Shoene et al., 2015; Thiede and
 556 Vasconcelos, 2010). In contrast, the Birimian is characterised by at least two >5 Ma pulses of
 557 basaltic magmatism, which are separated by ~35 Myr (Fig. 12, Abouchami et al., 1990; Sylvester
 558 and Attoh, 1992; Vidal and Alric, 1993; Dampare et al., 2008; Baratoux et al., 2011). Furthermore,
 559 as shown here, emplacement of evolved granitic rocks (PK105, West Accra biotite hornblende
 560 granodiorite) predates the mafic-ultramafic volcanism in the Birimian terrane, which contradicts the
 561 hypothesis of a plume-initiated growth cycle (Fig. 12). Our new zircon isotope data also negate the
 562 hypothesis presented by Boher et al. (1992), suggesting assimilation of older crust during anatexis,
 563 and crust generation in close proximity to existing continental crust.
 564 The available literature data for Birimian rocks have somewhat contrasting geochemical signatures,
 565 where mafic rocks are akin to ocean floor basalt, while the felsic rocks are dominated by magnesian
 566 granitic rocks with arc-like trace element signatures. To this end, it is worth noting that
 567 discriminating tectonic setting solely based on geochemical signatures has shortcomings unless
 568 these signatures are uniquely linked to physical processes (e.g. Hawkesworth and Scherstén, 2007).
 569 Nevertheless, taking chronological and geochemical data into account, the ocean plateau model
 570 proposed by Boher et al. (1992) seems untenable as the mafic magmatism is preceded and
 571 interleaved by calc-alkaline, magnesian felsic magmatism. By modern analogy, the mafic plateau-

building stage should rather have been represented by a short period with a large volume eruptive phase that preceded felsic magmatism. The alternative arc accretion model (Sylvester and Attoh, 1992; Feybesse and Milési, 1994; Ama-Salah, et al. 1996; Pouclet et al., 2006; Baratoux et al., 2011; de Kock et al., 2012) is more in line with available data, where some of the mafic magmatic stages might represent extensional periods of back-arc magmatism.

6.5. Alternating tectonics during crustal growth of the Birimian terrane

The temporal ϵHf -trends can be put into a plate tectonic framework with eastward subduction in a predominantly retreating arc system (Fig. 13). It is envisaged that juvenile island arc magmatism dominates between ~ 2.35 – 2.20 Ga (Fig. 13a). During this time period the West Accra granodiorite, PK105 crystallised (Fig. 12). Accretion of this island arc system to an assumed Archaean crust between ~ 2.18 – 2.13 Ga led to the crystallisation of PK102, ASGH007A, PK103 and PK101 (Fig. 13b). The ~ 2.18 – 2.13 Ga magmatism incorporates crust from an assumed Archaean terrane to the east as reflected by the subchondritic Hf isotope signatures seen in figure 12. The 2.17 Ga Nsawam biotite hornblende granite (PK102) has slightly less depleted ϵHf values than the contemporaneous Dixcove tonalite (ASGH007A) to the west (Figs. 12 and 13b). These differences might reflect trench-ward magmatism without reworked Archaean crust in the Dixcove tonalite while retro-arc magmatism to the east might have involved reworked Archaean crust. The pronounced Archaean influence between 2.141–2.126 Ga, as seen in the Gomoa Fetteh hornblende biotite granite (PK103) and the Amasaman biotite hornblende tonalite (PK101) samples (Fig. 12), coincides with the peak in Birimian crystallisation ages and argues for a continental setting during emplacement of these rocks. At ~ 2.13 Ga the main Eburnean orogeny began (Leube et al., 1990; Eisenlohr and Hirdes, 1992; Hirdes and Davis, 1998; Feybesse et al., 2006), and between 2.15–2.10 Ga several basins formed during an extensional phase (Feybesse et al., 2006), potentially explaining the abrupt return to supra-chondritic Hf-isotope signatures (Fig. 13c–d). This stage might have been associated with slab retreat and trench-ward magmatic migration from a thickened retro-arc into the thinned

extension zone where mantle derived magmas mix with juvenile continental crust generating melts with juvenile Hf isotope signatures (Kemp et al. 2009). Alternatively, crustal thickening during the closure of oceanic back-arcs can bury metasedimentary rocks derived from the Craton that melt during a subsequent extensional phase, giving rise to distinct but brief (<50 Myr) excursions toward negative Hf isotopic signatures (Bahlburg et al., 2009; Kemp et al. 2009; Mišković and Schaltegger, 2009; Collins et al., 2011). Such a scenario would, however, require the Archaean source to derive from sedimentary rocks, and all detrital zircon grains with sub-chondritic Hf isotope signatures reported by Kristinsdóttir, (2013) have more or less mantle oxygen signatures, suggesting that the Archaean crust never interacted with the hydrosphere. It is also noteworthy that samples with sub-chondritic Hf isotope signatures in this study are hornblende-bearing (metaluminous) granites, arguing against a S-type origin. Although intrusions that are younger than 2.13 Ga are relatively radiogenic for Hf (Fig. 12), they likely contain a component of ~2.3–2.2 Ga juvenile crust, as they host abundant metasediment xenoliths and are two-mica granites with a strong peraluminous signature.

7. Conclusions

The contribution from Archaean crust to the Birimian terrane is greater than previously known and comprises not only the Winneba pluton but also larger parts of the Kibi-Winneba belt as well as rocks intruding the Suhum basin. Reworking of Archaean crust was active during a short time period between ~2.14–2.13 Ga, where preceding and subsequent magmatism has relatively juvenile character.

The 2.23 Ga age of the West Accra granodiorite (PK105) requires the emplacement of felsic crust during the Eoeburnean and pre-dates suggested plume related rocks of Abuchami et al. (1990) and Boher et al. (1992) contradicting a suggested plume-initiated crustal growth stage.

An eastward, mainly retreating arc system with a shorter pulse of accretion between ~2.18–2.13 Ga and a rapid return to slab retreat explains trends seen in the combined zircon U-Pb and Lu-Hf isotope data and the geographical propagation of Archaean contribution to Birimian rocks.

Financial support provided by the Swedish Research Council (grant VR#2008-3447 and VR#2012-4531 to A. Scherstén), and by Per Westlings minnesfond to A. Petersson, are gratefully acknowledged. TK acknowledges ARC grant DP0773029. AS, PK and SA are grateful for the excellent driving and field support provided by Kwasi. Nordsim facility is operated under an agreement between the research funding agencies of Denmark, Norway and Sweden, the Geological Survey of Finland and the Swedish Museum of Natural History. Thanks go to M. Whitehouse at the Nordsim laboratory for reducing zircon U-Pb analytical data, L. Ilyinsky for assistance during ion probe analysis and to K. Lindén for preparation of ion probe mounts.

This is Nordsim contribution #XXX.

References

- Abati, J., Aghzer, A.M., Gerdes, A., Ennih, N., 2012. Insights on the crustal evolution of the West African Craton from Hf isotopes in detrital zircons from the Anti-Atlas belt. *Precambrian Research* 212–213, 263–274.
<http://dx.doi.org/10.1016/j.precamres.2012.06.005>
- Abouachami, W., Boher, M., Michard, A., Albarede, F., 1990. A major 2.1 Ga event of mafic magmatism in West Africa: An early stage of crustal accretion. *Journal of Geophysical Research* 95, 17605–17629.

- 647 Affaton, P., Rahaman, M.A., Trompette, R., Sougy, J., 1991. The Dahomeyide Orogen:
 648 tectonothermal evolution and relationships with the Volta basin. *In* R.D. Dallmeyer, J.P. Lecorche
 649 (Eds.), *The West African Orogens and Circum-Atlantic Correlatives*, Springer, Berlin, pp. 107–122
 650
- 651 Agyei Duodu, J., Loh, G.K., Hirdes, W., Boamah, K.O., Baba, M., Anokwa, Y.M., Asare, C.,
 652 Brako-hiapa, E., Mensah, R.B., Okla, R., Toloczyki, M., Davis, D.W., Glück, S., 2009. Geological
 653 Map of Ghana 1:1000000. BGS/GGS, Accra, Ghana/Hannover, Germany.
 654
- 655 Ama-Salah, I., Liégeois, J.-P., Pouclet, A., 1996: Evolution d'un arc insulaire océanique birimien
 656 précoce au Liptako nigérien (Sirba): géologie, géochronologie et géochimie. *Journal of African*
 657 *Earth Sciences*, 22, 235–254.
 658
- 659 Arndt, N.T., 2013. Formation and Evolution of the Continental Crust. *Geochemical Perspectives* 2,
 660 405–530.
 661
- 662 Attoh, K., Ekwueme, B.N., 1997. The West African Shield. *In*: de Wit, M. and Ashwal, L.D. (eds.)
 663 *Greenstone belts*. Oxford University Press, 517–528.
 664
- 665 Bahlburg, H., Vervoort, J.D., Du Frane, S.A., Bock, B., Augustsson, C., Reimann, C. 2009. Timing
 666 of crust formation and recycling in accretionary orogens: Insights learned from the western margin
 667 of South America. *Earth Science Reviews* 97, 215–241.
 668
- 669 Baratoux, L., Metelka, V., Naba, S., Jessell, M.W., Grégoire, M., Ganne, J., 2011. Juvenile
 670 Paleoproterozoic crust evolution during the Eburnean orogeny (2.2–2.0 Ga), western Burkina Faso.
 671 *Precambrian Research* 191, 18–45.
 672

- 673 Ben Othman, D., Polvé, M., Allègre, C.J., 1984. Nd-Sr isotopic composition of granulites and
674 constraints on the evolution of the lower continental crust, *Nature*, 307, 510–515, 1984.
- 675
- 676 Belousova, E. A., Kostitsyn, Y. A., Griffin, W. L., Begg, G. C., O'Reilly, S. Y., Pearson, N. J.,
677 2010. The growth of the continental crust: constraints from zircon Hf-isotope data. *Lithos*, 119,
678 457–466.
- 679
- 680 Blichert-Toft, J., Albarède, F., Rosing, M., Frei, R., Bridgwater, D. 1999. The Nd and Hf isotopic
681 evolution of the mantle through the Archean. results from the Isua supracrustals, West Greenland,
682 and from the Birimian terranes of West Africa. *Geochimica et Cosmochimica Acta* 63, 22, 3901–
683 3914.
- 684
- 685 Boher, M., Abouchami, W., Michard, A., Albarède, F., Arndt, N.T., 1992: Crustal growth in West
686 Africa at 2.1 Ga. *Journal of Geophysical Research* 97, 345–369.
- 687
- 688 Bouvier, A., Vervoort, J.D., Patchett, P.J., 2008. The Lu-Hf and Sm-Nd isotopic composition of
689 CHUR: constraints from unequilibrated chondrites and implication for the bulk composition of
690 terrestrial planets. *Earth and Planetary Science Letters* 273, 48–57.
- 691
- 692 Collins, W.J., Belousova, E.A., Kemp, A.I.S., Murphy, J.B. 2011. Two contrasting Phanerozoic
693 orogenic systems revealed by hafnium isotope data. *Nature Geoscience* 4, 333–337.
694 doi: 10.1038/NGEO1127
- 695
- 696 Condie, K.C., O'Neill, C., Aster, R.C. 2009. Evidence and implications for widespread magmatic
697 shutdown for 250 My on Earth. *Earth and Planetary Science Letters* 282. 294–298.
- 698

- 699 Davies, D.W., Hirdes, W., Schaltegger, U., Nunoo, E.A., 1994. U-Pb age constraints on deposition
700 and provenance of Birimian and gold-bearing Tarkwaian sediments in Ghana, West Africa.
701 *Precambrian Research* 67, 89–107.
- 702
- 703 de Kock, G.S, Botha, P.M.W., Théveniaut, H., Gyapong, W., 2009. Geological Map Explanation –
704 Map Sheet 0803B (1:100 000), CGS/BRGM/Geoman Geological Survey Department of Ghana
705 (GSD), N° MSSP/2005/GSD/1^a.
- 706
- 707 de Kock, G.S., Armstrong, R.A., Siegfried, H.P., Thomas, E., 2011. Geochronology of the Birim
708 Supergroup of the West African Craton in the Wa-Bolé region of west-central Ghana: Implications
709 for the stratigraphic framework. *Journal of African Earth Sciences*, 59, 1–40.
710 doi:10.1016/j.jafrearsci.2010.08.001
- 711
- 712 de Kock, G.S., Théveniaut, H., Botha, P.M.W., Gyapong, W., 2012. Timing the structural events in
713 the Paleoproterozoic Bolé-Nangodi belt terrane and adjacent Maluwe basin, West African Craton,
714 in central-west Ghana. *Journal of African Earth Sciences* 65, 1–24.
- 715
- 716 Dhuime, B., Hawkesworth, C., Cawood, P. 2011. When continents formed. *Science* 331, 154–155.
- 717
- 718 Dhuime, B., Hawkesworth, C., Cawood, P., Storey, C.D. 2012. A Change in the Geodynamics of
719 Continental Growth 3 Billion Years Ago. *Science* 335, 1334–1336.
720 doi: 10.1126/science.1216066
- 721
- 722 Doumbia, S., Pouclet, A., Kouamelan, A., Peucat, J.J., Vidal, M., Delor, C., 1998: Petrogenesis of
723 juvenile-type Birimian (Paleoproterozoic) granitoids in central Côte d’Ivoire, West Africa:
724 geochemistry and geochronology. *Precambrian Research* 87, 33–63.

725

726 Egal, E., Thiéblemont, D., Lahondère, D., Guerrot, C., Costea, C.A., Iliescu, D., Delor, D., Goujou,
 727 J-C., Lafon, J.M., Tegye, M., Diaby, S., Kolié, P., 2002. Late Eburnean granitization and tectonics
 728 along the western and northwestern margin of the Archean Kénéma-Man domain (Guinea, West
 729 African Craton). *Precambrian Research* 117, 57–84.

730

731 Ennih, N., Liégeois, J.P., 2008. The boundaries of the West African Craton, with special reference
 732 to the basement of the Moroccan metaCratonic Anti-Atlas belt. *In* N. Ennih and J.P. Liégeois (eds.):
 733 The boundaries of the West African Craton, 1–17. The Geological Society of London Special
 734 Publication 297.

735

736 Evans, M.J., Attah, K., White, W.M. 1996. REE and HFSE concentrations in Early Proterozoic
 737 greenstone belts of West Africa: Implications for oceanic plateau vs. Arc accretion in juvenile crust
 738 production. *EOS Transactions of American Geophysical Union* 77, S291.

739

740 Feybesse, J.L., Milési, J.-P., 1994: The Archean/Paleoproterozoic contact zone in West Africa: a
 741 mountain belt of décollement thrusting and folding on a continental margin related to 2.1 Ga
 742 convergence of Archean Cratons? *Precambrian Research* 69, 199–227.

743

744 Feybesse, J.L., Billa, M., Guerrot, C., Duguey, E., Lescuyer, J.L., Milési, J.P., Bouchot, V., 2006:
 745 The Paleoproterozoic Ghanaian province: Geodynamic model and ore controls, including regional
 746 stress modeling. *Precambrian Research* 149, 149–196.

747

748 Fisher, C.M., Hanchar, J.M., Samson, S.D., Dhuime, B., Blichert-Torft, J., Vervoort, J.D., Lam, R.,
 749 2011. Synthetic zircon doped with hafnium and rare earth elements: a reference material for in situ
 750 hafni-um isotope analysis. *Chemical Geology* 286, 32–47.

751

752 Gasquet, D., Barbey, P., Adou, M., Paquette, J.L., 2003. Structure, Sr-Nd isotope geochemistry and
753 zircon U-Pb geochronology of the granitoids of the Dabakala area (Côte d'Ivoire): evidence for a
754 2.3 Ga crustal growth event in the Paleoproterozoic of West Africa? *Precambrian Research* 127,
755 329–354.

756

757 Gerdes, A., Zeh, A., 2006. Combined U-Pb and Hf isotope LA-(MC)-ICP-MS analyses of
758 detrital zircons: Comparison with SHRIMP and new constraints for the provenance and
759 age of an Armorican metasediment in Central Germany. *Earth and Planetary Sciences Letters* 249,
760 47–61.

761

762 Gerdes, A., Zeh, A., 2009. Zircon formation versus zircon alteration — New insights from
763 combined U-Pb and Lu-Hf in-situ LA-ICP-MS analyses, and consequences for the interpretation of
764 Archean zircon from the Central Zone of the Limpopo Belt. *Chemical Geology* 261, 230–243.
765 doi:10.1016/j.chemgeo.2008.03.005

766

767 Gueye, M., Siegesmund, S., Wemmer, K., Pawlig, S., Drobe, M., Nolte, N., Layer, P., 2007. New
768 evidences for an early Birimian evolution in the West African Craton: An example from the
769 Kedougou-Kéniéba inlier, southeast Senegal. *South African Journal of Geology* 110, 511–534.

770

771 Grenholm, 2014. Grenholm, M., The Birimian event in the Baoulé Mossi domain (West African
772 Craton) — regional and global context. Master thesis in Geology, Lund University - Lithosphere
773 and Paleobiosphere Sciences, no. 375. (45 hskp/ECTS).

774

775 Griffin, W.L., Pearson, N.J., Belousova, E., Jackson, S.E., van Achterbergh, E., O'Reilly, S.Y.,
776 Shee, S.R. 2000. The Hf isotope composition of Cratonic mantle: LAM-MC-ICPMS analysis of

zircon megacrysts in kimberlites. *Geochemica et Cosmica Acta* 64, 1, 133–147.

[http://dx.doi.org/10.1016/S0016-7037\(99\)00343-9](http://dx.doi.org/10.1016/S0016-7037(99)00343-9)

Hawkesworth, C., Scherstén, A., 2007. Mantle plumes and geochemistry. *Chemical Geology* 241, 319–331.

Hawkesworth, C., Turner, S., Peate, D., McDermott, F. van Calsteren, P., 1997. Elemental U and Th variations in island arc rocks: implications for U-series isotopes. *Chemical Geology* 139, 207–221.

Hawkesworth, C., Cawood, P., Kemp, T., Storey, C., Dhuime, B. 2009. A matter of preservation. *Science* 323. 49–50.

Hawkesworth, C.J., Dhuime, B., Pietranik, A.B., Cawood, P.A., Kemp, A.I.S., Storey, C.D. 2010. The generation and evolution of the continental crust. *Journal of the Geological Society, London* 167, 229–248.
doi: 10.1144/0016-76492009-072.

Hiess, J., Bennett, V. C., Nutman, A. P., Williams, I. S., 2011. Archaean fluid-assisted crustal cannibalism recorded by low $\delta^{18}\text{O}$ and negative $\epsilon_{\text{Hf}}(\text{T})$ isotopic signatures of West Greenland granite zircon. *Contributions to Mineralogy and Petrology*, 161, 1027–1050.

Hirdes., Davis, D.W., Eisenlohr, B.N., 1992. Reassessment of Proterozoic granitoid ages in Ghana on the basis of U/Pb zircon and monazite dating. *Precambrian Research*, 56, 89–96.

- Hirdes, W., Davis, D.W., 1998. First U-Pb zircon age extrusive volcanism in the Birimian Supergroup of Ghana, West Africa. *Journal of African Earth Sciences* 27, 291–294.
- Hirdes, W., Davis, D.W., 2002. U-Pb geochronology of Paleoproterozoic rocks in the southern part of the Kedougou-Kéniéba Inlier, Senegal, West Africa: Evidence for diachronous accretionary development of the Eburnean Province. *Precambrian Research* 118, 83–99.
- Hirdes, W., Davis, D.W., Lüdtke, G., Konan, G., 1996. Two generations of Birimian (Paleoproterozoic) volcanic belts in northeastern Côte d’Ivoire (West Africa): Consequences for the “Birimian controversy”. *Precambrian Research* 80, 173–191.
- Iizuka, T., Campbell, I.H., Allen, C.M., Gill, J.B., Maruyama, S., Makoka, F., 2013. Evolution of the African continental crust as recorded by U-Pb, Lu-Hf and O isotopes in detrital zircons from modern rivers. *Geochimica et Cosmochimica Acta* 107, 96–120.
- Kemp, A. I. S., Whitehouse, M. J., Hawkesworth, C. J., Alarcon, M. K., 2005. A zircon U-Pb study of metaluminous (I-type) granites of the Lachlan Fold Belt, southeastern Australia: Implications for the high/low temperature classification and magma differentiation processes. *Contributions to Mineralogy and Petrology*, 150, 230–249.
- Kemp, A.I.S., Hawkesworth, C.J., Collins, W.J., Gray, C.M., Belvin, P.L., EIMF. 2009. Isotopic evidence for rapid continental growth in an extensional accretionary orogen: The Tasmanides, eastern Australia. *Earth and Planetary Science Letters*, 284, 455–466.
doi:10.1016/j.epsl.2009.05.011.

- 827 Kristinsdóttir, B., Scherstén, A., Kemp, A.I.S., Petersson, A., 2013. Juvenile Crustal Growth during
 828 the Palaeoproterozoic: U-Pb-O-Hf Isotopes of Detrital Zircon from Ghana. *Mineralogical Magazine*
 829 77, (5), 1513.
- 830
- 831 Klein, E.L., Luzardo, R., Moura, C.A.V., Armstrong, R., 2008. Geochemistry and zircon
 832 geochronology of Paleoproterozoic granitoids: Further evidence on the magmatic and crustal
 833 evolution of the Sao Luis Cratonic fragment, Brazil. *Precambrian Research*, 165, 221–242.
- 834
- 835 Lahondère, D., Thiéblemont, D., Tegye, M., Guerrot, C., Diabate, B. 2002. First evidence of early
 836 Birimian (2.21 Ga) volcanic activity in Upper Guinea: the volcanics and associated rocks of the
 837 Niani suite. *Journal of African Earth Sciences* 35. 417–431.
- 838
- 839 Layton, W., 1958. The geology of 1/4° field sheet 32. Ghana Geological Survey, Bulletin 24, 66 pp.
- 840
- 841 Leube, A., Hirdes, W., Mauer, R., Kesse, G.O., 1990. The early Proterozoic Birimian Supergroup of
 842 Ghana and some aspects of its associated gold mineralization. *Precambrian Research*, 46, 139–165.
- 843
- 844 Liégeois, J.P., Claessens, W., Camara, D., Klerkx, J., 1991: Short-lived Eburnian orogeny in
 845 southern Mali. *Geology, tectonics, U-Pb and Rb-Sr geochronology. Precambrian Research*, 50,
 846 111–136.
- 847
- 848 Linnemann, U., Gerdes, A., Hofmann, M., Marko, L., 2014. The Cadomian Orogen:
 849 Neoproterozoic to Early Cambrian crustal growth and orogenic zoning along the periphery of the
 850 West African Craton—Constraints from U–Pb zircon ages and Hf isotopes (Schwarzburg Antiform,
 851 Germany). *Precambrian Research* 244, 236–278.
- 852 <http://dx.doi.org/10.1016/j.precamres.2013.08.007>

853

854 Lompo, M., 2009. Geodynamic evolution of the 2.25-2.0 Ga Paleoproterozoic magmatic rocks in
 855 the Man-Leo shield of the West African Craton. A model of subsidence of an oceanic plateau. *In*:
 856 S.M. Reddy, R. Mazumder, D.A.D. Evans, A.S. Collins (eds.): Paleoproterozoic supercontinents
 857 and global evolution, 231–254. The Geological Society of London Special Publication 323.

858

859 Lompo, M., 2010. Paleoproterozoic structural evolution of the Man-Leo shield (West Africa). Key
 860 structures for vertical and transcurrent tectonics. *Journal of African Earth Sciences* 58. 19–36.

861

862 Ludwig, K. R., 2008. Isoplot 3.70. A geochronological toolkit for Microsoft Excel. Berkeley
 863 Geochron. Center Spec. Pub., 4.

864

865 McFarlane, C.R.M., Mavrogenes, J., Lentz, D., King, K., Allibone, A., Holcombe, R. 2011.
 866 Geology and intrusion-related affinity of the Morila gold mine, southeast Mali. *Economic Geology*
 867 106. 727–750.

868

869 McGee, L.E., Smith, I.E.M., Millet, M.-A., Handley, H.K., Lindsay, J.M., 2013. Asthenospheric
 870 Control of Melting Processes in a Monogenetic Basaltic System: a Case Study of the Auckland
 871 Volcanic Field, New Zealand, *Journal of Petrology* 54, 10, 2125–2153.

872

873 Milési, J.P., Feybesse, J.L., Ledru, P., Dommanget, A., Ouedraogo, M.F., Tegye, M., Calvez, J.Y.,
 874 Lagny, P., 1989. Les minéralisations aurifères de l'Afrique de l'Ouest; leur evolution
 875 lithostructurale au Protérozoïque inférieur. *Chronique de la Recherche Minière* 497, 3–98.

876

- 877 Mišković, A., Schaltegger, U. 2009. Crustal growth along a non-collisional Cratonic margin: A
878 LuHf isotopic survey of the Eastern Cordilleran granitoids of Peru. *Earth and Planetary Science*
879 *Letters* 279, 303–315.
- 880
- 881 Næraa, T., Scherstén, A., Rosing, M.T., Kemp, A.I.S., Hoffman, J.E., Kockfelt, T.F., Whitehouse,
882 M.J. 2012. Hafnium isotope evidence for a transition in the dynamics of continental growth 3.2Gyr
883 ago. *Nature* 485, 627–630.
884 doi:10.1038/nature11140
- 885
- 886 Næraa, T., Kemp, A. I. S., Scherstén, A., Rehnström, E. F., Rosing, M. T., Whitehouse, M. J., 2014.
887 A lower crustal mafic source for the ca. 2550Ma Qôrqu Granite Complex in southern West
888 Greenland. *Lithos*, 192, 291–304.
- 889
- 890 Partin. C.A., Bekker, A., Sylvester, P.J., Wodicka, N., Stern, R.A., Chacko, T., Heaman, L.M.,
891 2014. Filling in the juvenile magmatic gap: Evidence for uninterrupted Paleoproterozoic
892 plate tectonics. *Earth and Planetary Science Letters* 388, 123–133.
- 893
- 894 Pawlig, S., Gueye, M., Klischies, R., Schwarz, S., Wemmer, K., Siegesmund, S., 2006.
895 Geochemical and Sr-Nd isotopic data on the Birimian of the Kedougou-Kéniéba Inlier (eastern
896 Senegal): Implications on the Paleoproterozoic evolution of the West African Craton. *South African*
897 *Journal of Geology*, 109, 411–427.
- 898
- 899 Persits, F., Ahlbrandt, T., Tuttle, M., Charpentier, R., Brownfield, M., Takahashi, K., 2002. Map
900 showing geology, oil and gas fields and geological provinces of Africa, ver. 2.0. USGS Open File
901 Report 97-470A.
902 <http://pubs.usgs.gov/of/1997/ofr-97-470/OF97-470A/index.html>, last accessed 06-07-2013.

903

904 Petersson, A., Scherstén, A., Andersson, J., Möller, C., 2015a. Zircon U–Pb and Hf–isotopes from
 905 the eastern part of the Sveconorwegian Orogen, SW Sweden: implications for the growth of
 906 Fennoscandia. *Geological Society, London, Special Publications*, 389, 281–303.

907

908 Petersson, A., Scherstén, A., Bingen, B., Gerdes, A., Whitehouse, M. J., 2015b. Mesoproterozoic
 909 continental growth: U–Pb–Hf–O zircon record in the Idefjorden Terrane, Sveconorwegian Orogen.
 910 *Precambrian Research*, 261, 75–95.

911

912 Peucat, J.-J., Capdevila, R., Drareni, A., Mahdjoub, Y., Kahoui, M., 2005. The Eglab massif in the
 913 West African Craton (Algeria), an original segment of Eburnean orogenic belt: Petrology
 914 geochemistry and geochronology. *Precambrian Research*, 136, 309–352.

915

916 Pouclet, A., Doumbia, S., Vidal, M., 2006. Geodynamic setting of the Birimian volcanism in central
 917 Ivory Coast (western Africa) and its place in the Palaeoproterozoic evolution of the Man shield.
 918 *Bulletin de la Societe Geologique de France*, 177, 105–121.

919

920 Scherer, E., Münker, C., Mezger, K., 2001. Calibration of the lutetium-hafnium clock. *Science* 293,
 921 683–687.

922

923 Schoene, B., Samperton, K.M., Eddy, M.P., Keller, G., Adatte, T., Bowring, S.A., Khadri, S.F.R.,
 924 Gertsch, B., 2015. U–Pb geochronology of the Deccan Traps and relation to the end-Cretaceous
 925 mass extinction. *Science* 347, 182–184.

926

927 Schofield, D.I., Horstwood, M.S.A., Pitfield, P.E.J., Gillespie, M., Darbyshire, F., O'Connor, E.A.,
 928 Abdouloye, T.B., 2012. U–Pb dating and Sm–Nd isotopic analysis of granitic rocks from the Tiris

Complex: New constraints on key events in the evolution of the Reguibat Shield, Mauritania.

Precambrian Research 204–205, 1–11.

Segal, I., Halicz, L., Platzner, I.T., 2003. Accurate isotope ratio measurements of ytterbium by multiple collector inductively coupled plasma mass spectrometry applying erbium and hafnium in an improved double external normalization procedure. *Journal of Analytical Atomic Spectrometry* 18, 1217–1223.

Siegfried, P., Aggenbach, A., Clarke, B., Delor, C., Yves Roig, J. 2009. Geological Map Explanation, Map Sheet 0903D (1:100 000). CGS/BRGM/Geoman. Geological Survey Department of Ghana.

Stacey, J.S., Kramers, J.D., 1975, Approximation of terrestrial lead isotope evolution by a 2-stage model. *Earth and Planetary Science Letters* 26, 207–221.

Steiger, R.H., Jäger, E., 1977, Subcommittee on geochronology: convention of the use of decay constants in geo- and cosmochemistry. *Earth and Planetary Science Letters* 36, 359–362.

Stein, M., Goldstein, S.L., 1996. From plume head to continental lithosphere in the Arabian–Nubian shield. *Nature* 382, 773–778.

Stern, C.R. 2011. Subduction erosion: Rates, mechanisms, and its role in arc magmatism and the evolution of the continental crust. *Gondwana Research* 20. 284–308.

- 953 Sylvester, P.J., Attah, K., 1992. Lithostrathigraphy and composition of 2.1 Ga greenstone belts of
954 the West African Craton and their bearing on crustal evolution and the Archean-Proterozoic
955 boundary. *Journal of Geology*, 100, 377–392.
- 956
- 957 Söderlund, U., Patchett, P.J., Vervoort, J.D., Isachsen, C.E., 2004. The ^{176}Lu decay constant deter-
958 mined by Lu-Hf and U-Pb isotope systematics of Precambrian mafic intrusions. *Earth and*
959 *Planetary Science Letters* 219, 311–324.
- 960
- 961 Tapsoba, B., Lo, C.-H., Jahn, B.-M., Chung, S.-L., Wenmenga, U., Iizuka, Y., 2013. Chemical and
962 Sr-Nd isotopic compositions and zircon U-Pb ages of the Birimian granitoids from NE Burkina
963 Faso, West African Craton: Implications on the geodynamic setting and crustal evolution.
964 *Precambrian Research*, 224, 364–396.
- 965
- 966 Taylor, P.N., Moorbath, S., Leube, A. and Hirdes, W., 1988. Geochronology and crustal evolution
967 of Early Proterozoic granite-greenstone terrains in Ghana/West Africa, Abstr., International
968 Conference on the Geology of Ghana with Special Emphasis on Gold Comm. 75th Anniversary of
969 Ghana Geological Survey. Department of Accra, pp. 43–45.
- 970
- 971 Taylor, P.N., Moorbath, S., Leube, A. and Hirdes, W., 1992. Early Proterozoic crustal evolution in
972 the Birimian of Ghana: constraints from geochronology and isotope geochemistry. *Precambrian*
973 *Research* 56, 97–111.
- 974
- 975 Thiede, D.S., Vasconcelos, P.M., 2010. Paraná flood basalts: Rapid extrusion hypothesis confirmed
976 by new $^{40}\text{Ar}/^{39}\text{Ar}$ results. *Geology* 38, (8), 747–750.
- 977

- 978 Thomas, E., Baglow, N., Viljoen, J., Siaka, Z., 2009. Geological Map Explanation, Map Sheet
 979 0903D (1:100 000). CGS/BRGM/Geoman. Geological Survey Department of Ghana.
 980
- 981 Vervoort, J.D., Plank, T., Prytulak, J., 2011. The Hf–Nd isotopic composition of marine sediments.
 982 *Geochimica et Cosmochimica Acta* 75, 20, 5903–5926.
 983
- 984 Vervoort, J.D., Patchett, P.J., Söderlund, U., Baker, M., 2004. Isotopic composition of Yb and the
 985 determination of Lu concentrations and Lu/Hf ratios by isotope dilution using MC-ICPMS.
 986 *Geochemistry, Geophysics, Geosystems* 5.
 987 doi: 10.1029/2004GC000721.
 988
- 989 Vidal, M., Alric, G., 1994: The Paleoproterozoic (Birimian) of Haute-Comoé in the West African
 990 Craton, Ivory Coast: A transtensional back-arc basin. *Precambrian Research*, 65, 207–229.
 991
- 992 Vidal, M., Delor, C., Pouclet, A., Simeon, Y., Alric, G. 1996. Evolution géodynamique de l’Afrique
 993 de l’Ouest entre 2.2 Ga et 2 Ga: Le style archéen des ceintures vertes et des ensembles
 994 sédimentaires birimiens du nord-est de la Côte-d’Ivoire. *Bulletin de la Societe Geologique de*
 995 *France* 167. 307–319.
 996
- 997 Vidal, M., Gumiaux, C., Cagnard, F., Pouclet, A., Ouattara, G., Pichon, M. 2009. Evolution of a
 998 Paleoproterozoic “weak type” orogeny in the West African Craton (Ivory Coast). *Tectonophysics*
 999 477. 145–159.
 1000
- 1001 Wiedenbeck, M., Hanchar, J.M., Peck, W.H., Sylvester, P., Valley, J., Whitehouse, M., Kronz, A.,
 1002 Morishita, Y., Nasdala, L., Fiebig, J., Franchi, I., Girard, J.-P., Greenwood, R.C., Hinton, R., Kita,
 1003 N., Mason, P.R.D., Norman, M., Ogasawara, M., Piccoli, P.M., Rhede, D., Satoh, H., Schulz-

Dobrick, B., Skar, O., Spicuzza, M.J., Terada, K., Tindle, A., Togashi, S., Vennemann, T., Xie, Q.,
Zheng, Y.-F., 2004. Further characterization of the 91500 zircon crystal. *Geostandards and*
Geoanalytical Research 28, 9–39.

Whitehouse, M. J., Kamber, B. S., 2005. Assigning dates to thin gneissic veins in high-grade
metamorphic terranes: a cautionary tale from Akilia, Southwest Greenland. *Journal of Petrology* 46,
291–318.

Whitehouse, M. J., Kamber, B. S., Moorbath, S., 1999. Age significance of U-Th-Pb zircon data
from early Archean rocks of west Greenland – a reassessment based on combined ion microprobe
and imaging studies. *Chemical Geology* 160, 210–224.

Whitehouse, M.J., Nemchin, A.A., 2009. High precision, high accuracy measurement of oxygen
isotopes in a large lunar zircon by SIMS, *Chemical Geology* 261, 32–42.

Woodhead, J.D., Hergt, J.M., 2005. A preliminary appraisal of seven natural zircon reference
materials for in situ Hf isotope determination. *Geostandards and Geoanalytical Research* 29, 183–
195.

Figure Captions

Fig. 1a. Simplified tectonic map of the West African Craton and adjacent Pan-African-Hercynian fold and thrust belts. Mesoproterozoic to recent sedimentary rocks are not depicted. The map has been compiled from the following sources; Man-Leo shield, Kedougou-Kéniéba, Kayes (Egal et al. 2002; Baratoux et al. 2011), Reguibat shield (Peucat et al. 2005; Schofield et al. 2012), Pan-African belts (Persits et al. 2002; Baratoux et al. 2011) and Hercynian belt (Abouchami et al. 1990; Schofield et al. 2012). WAC boundaries after Ennih and Liégeois (2008). Redrawn after Grenholm (2014).

1b. Schematic geological map of Birimian rocks of the Man-Leo shield redrawn after Baratoux et al. (2011) with modifications by Egal et al. (2002), Agyei Duodu et al. (2009) and Grenholm (2013). Key to inherited zircon: 1: Gondo granite gneiss, EC1074A, 2.876 Ga and 2.499 Ga, Thomas et al. (2009). 2: Ifantayire granite gneiss, SC1011, 2.386 Ga and 2.258 Ga, Siegfried et al. (2009). 3: Dabakala tonalitic gneiss, s8-32, 2.312 Ga, Gasquet et al. (2003). 4: Gomoa Fetteh hornblende biotite granite, PK103, 2.460 Ga, this study.

1c. Geological map of Ghana showing sample locations, basins, belts and main rock units. Initial version of the map was compiled by Watts, Griffit and McQuat Ltd, Lakewood Colorado, USA.

Fig. 2. Small samples aliquot (left) showing macroscopic features. Plane polarised thin section view (ppl) of a representative area (middle). Cross polarised thin section view (xpl) of the same area as for the plane polarised view (right).

Fig. 3. BSE (Back-Scattered-Electrone) image of representative zircon grains. Ellipses indicate spot locations, small thin: U-Pb and large thick: Lu-Hf. Numbers inside U-Pb ellipses refer to analytical ID in U-Pb and Lu-Hf data tables. Dashed ellipses and results in italic denote discarded analyses.

Fig. 4. BSE (Back-Scattered-Electrone) image of representative zircon grains. Ellipses indicate spot locations, small thin: U-Pb and large thick: Lu-Hf. Numbers inside U-Pb ellipses refer to analytical ID in U-Pb and Lu-Hf data tables. Dashed ellipses and results in italic denote discarded analyses.

Fig. 5. BSE (Back-Scattered-Electrone) image of representative zircon grains. Ellipses indicate spot locations, small thin: U-Pb and large thick: Lu-Hf. Numbers inside U-Pb ellipses refer to analytical ID in U-Pb and Lu-Hf data tables. Dashed ellipses and results in italic denote discarded analyses.

Fig. 6. BSE (Back-Scattered-Electrone) image of representative zircon grains. Ellipses indicate spot locations, small thin: U-Pb and large thick: Lu-Hf. Numbers inside U-Pb ellipses refer to analytical ID in U-Pb and Lu-Hf data tables. Dashed ellipses and results in italic denote discarded analyses.

Fig. 7. BSE (Back-Scattered-Electrone) image of representative zircon grains. Ellipses indicate spot locations, small thin: U-Pb and large thick: Lu-Hf. Numbers inside U-Pb ellipses refer to analytical ID in U-Pb and Lu-Hf data tables. Dashed ellipses and results in italic denote discarded analyses.

Fig. 8. BSE (Back-Scattered-Electrone) image of representative zircon grains. Ellipses indicate spot locations, small thin: U-Pb and large thick: Lu-Hf. Numbers inside U-Pb ellipses refer to analytical ID in U-Pb and Lu-Hf data tables. Dashed ellipses and results in italic denote discarded analyses.

Fig. 9. BSE (Back-Scattered-Electrone) image of representative zircon grains. Ellipses indicate spot locations, small thin: U-Pb and large thick: Lu-Hf. Numbers inside U-Pb ellipses refer to analytical ID in U-Pb and Lu-Hf data tables. Dashed ellipses and results in italic denote discarded analyses.

Fig. 10. BSE (Back-Scattered-Electrone) image of representative zircon grains. Ellipses indicate spot locations, small thin: U-Pb and large thick: Lu-Hf. Numbers inside U-Pb ellipses refer to analytical ID in U-Pb and Lu-Hf data tables. Dashed ellipses and results in italic denote discarded analyses.

Fig. 11. Tera-Wasserburg concordia diagrams showing SIMS (Secondary-Ion-Mass-Spectrometry) zircon spot data for all samples (± 2 error ellipses) and obtained ages. All ages are shown with 2 errors. Red ellipses denote discarded analyses not used in age calculation. Dashed lines denote discordia lines.

Fig. 12. ϵ Hf versus crystallisation ages (in Ma). ϵ Hf has been calculated using current CHUR values of $^{176}\text{Hf}/^{177}\text{Hf}$. 0.282785 and $^{176}\text{Lu}/^{177}\text{Hf}$. 0.0336 from Bouvier et al. (2008). ^{176}Lu decay constants of Söderlund et al. (2004) and Scherer et al. (2001) were used in all calculations. Ages represent interpreted igneous crystallisation ages for individual samples. ϵ Hf-value of the Winneba pluton corresponds to the recalculated Nd-isotope data of Taylor et al. (1990), including age error bars.

Vertical grey lines represent timing of reported mafic volcanism in the Baoulé Mossi domain (Abouchami et al., 1990; Sylvester and Attah, 1992; Vidal and Alric, 1993; Dampare et al., 2008; Baratoux et al., 2011).

Fig. 13. Theoretical evolutionary model proposed for the arc system generating the Birimian terrane in Ghana. A. Retreating eastward subduction generating juvenile island arc magmatism outboard

the Western Archaean crust. B. Switch to an advancing arc system with accretion of the juvenile island arcs onto the eastern Archaean crust. ~2.18–2.13 Ga magmatism incorporates crust from the Archaean nucleus to the east as reflected in subchondritic Hf-isotope signatures. C. Slab retreat migrates igneous activity trench-ward from the thickened back arc into the thinned extension zone where mantle derived magmas mix with juvenile continental crust. D. Continued extensional tectonic regime and simultaneous amalgamation of the Birimian crust to the western Archaean Man-Shield.

Supplementary figure A.1. Mean values of standard runs during Hf-isotope analyses presented in $^{176}\text{Hf}/^{177}\text{Hf}$. Data quality was controlled using standards Mud Tank, FC-1 (Woodhead and Hergt 2005) and synthetic zircon (Fisher et al. 2011).

Table 1. U-Pb

Sample	[Pb]	[U]	Th/U	²⁰⁶ Pb/ ²³⁸ U	²⁰⁷ Pb/ ²³⁵ U	²⁰⁶ Pb/ ²³⁸ U	±σ	²⁰⁷ Pb/ ²³⁵ U	±σ	%Disc ^c	²⁰⁶ Pb/ ²³⁸ U	±σ	²⁰⁷ Pb/ ²³⁵ U	±σ	εHF	±2σ
Spot # ^a	ppm	ppm	calc.		%					2σ-limit	age (Ma)		age (Ma)			
PK101																
n3762-01	176.0	628.0	0.40	702	2.67	4.645	0.9	0.11756	0.6	-35.1	1257	11	1919	10		
n3762-02	155.0	381.0	0.65	12576	0.15	3.336	0.9	0.12627	0.4	-17.6	1690	14	2047	6		
n3762-03	235.0	562.0	1.29	124	15.14	4.011	2.7	0.12593	11.7		1435	34	2042	194		
n3762-04	181.0	495.0	0.30	6414	0.29	3.359	1.5	0.12411	0.5	-15.7	1680	22	2016	9		
n3762-05	153.0	278.0	0.84	89593	0.02	2.476	1.0	0.13320	0.5		2187	18	2141	8	-4.5	0.7
n3762-06	145.0	327.0	0.32	15848	0.12	2.760	0.9	0.13033	0.3	-3.7	1993	16	2102	6	-3.2	0.7
n3762-07	138.0	324.0	0.30	633	2.96	2.875	1.0	0.13108	0.7	-7.0	1924	16	2112	12	-2.0	1.6
n3762-08	205.0	567.0	0.62	6482	0.29	3.777	0.9	0.12280	0.3	-25.1	1514	13	1997	6		
n3762-09	153.0	322.0	0.45	60587	0.03	2.651	1.0	0.13094	0.3	-0.3	2063	17	2111	6	-1.6	1.4
n3762-10	144.0	322.0	0.58	2695	0.69	2.950	0.9	0.12998	0.4	-8.8	1882	15	2084	7		
n3762-11	171.0	418.0	0.39	7133	0.26	3.088	0.9	0.12773	0.3	-12.2	1806	15	2067	6		
n3762-12	123.0	267.0	0.19	18907	0.10	2.584	0.9	0.13178	0.4		2109	17	2122	6	-3.4	1.5
n3762-13	174.0	363.0	0.56	31339	0.06	2.716	0.9	0.13145	0.3	-3.0	2021	16	2117	6	-2.8	0.6
n3762-14	137.0	281.0	0.56	15095	0.12	2.667	1.0	0.13236	0.4	-1.6	2053	18	2129	7	-3.7	0.6
n3762-15	199.0	528.0	0.07	7064	0.26	3.046	1.7	0.12688	0.3	-9.3	1830	28	2055	6	-3.1	0.7
PK102																
n3689-01	223.0	425.0	0.59	134449	0.01	2.487	0.8	0.13667	0.2		2179	15	2185	4	3.0	6.7
n3689-02	91.0	179.0	0.49	66738	0.03	2.499	0.6	0.13615	0.3		2170	11	2179	5	2.6	6.3
n3689-03	127.0	250.0	0.49	127665	0.01	2.501	0.6	0.13457	0.3		2168	11	2159	5	1.4	5.2
n3689-HF-03b															2.0	0.5
n3689-04	86.0	170.0	0.43	113671	0.02	2.492	0.6	0.13583	0.3		2175	12	2175	6	2.8	6.5
n3689-05	118.0	244.0	0.37	55465	0.03	2.563	0.6	0.13455	0.3	-0.2	2124	11	2158	5	3.4	7.1
n3689-06	95.0	186.0	0.47	53676	0.03	2.461	0.7	0.13575	0.3		2198	13	2174	5	3.0	6.7
n3689-07	102.0	204.0	0.43	92483	0.02	2.526	0.6	0.13636	0.3		2150	12	2182	5	2.0	5.7
n3689-08	175.0	342.0	0.46	201430	0.01	2.472	0.6	0.13613	0.2		2190	12	2179	4	0.8	4.5
n3689-09	223.0	545.0	0.37	13560	0.14	3.078	1.3	0.13097	0.3	-13.7	1813	20	2111	5	1.5	5.2
n3689-10	152.0	324.0	0.39	49225	0.04	2.663	0.6	0.13434	0.2	-3.9	2056	11	2156	4	5.3	9.0
n3689-11	85.0	167.0	0.49	37157	0.05	2.503	0.6	0.13541	0.3		2167	11	2169	6	2.1	5.8
n3689-12	136.0	337.0	0.30	13495	0.14	3.055	0.6	0.13168	0.3	-14.2	1826	10	2121	6		
n3689-13	93.0	182.0	0.38	281785	0.01	2.428	0.6	0.13647	0.3	0.3	2224	12	2183	6	1.4	5.1
n3689-14	61.0	157.0	0.48	45098	0.04	2.465	0.6	0.13483	0.3		2195	12	2162	6	2.9	6.6
n3689-15	107.0	210.0	0.42	238742	0.01	2.467	0.6	0.13638	0.3		2193	11	2182	5	3.0	6.7
n3689-16	78.0	150.0	0.50	>1x10 ⁵	0.00	2.467	0.6	0.13622	0.3		2193	11	2180	6	3.0	6.7
n3689-HF-17															3.7	0.6
n3689-HF-18															1.1	0.8
n3689-HF-19															2.6	0.5
PK103																
n3763-01	127.0	251.0	0.50	85446	0.02	2.520	1.0	0.13407	0.4		2154	18	2152	6	1.7	0.5
n3763-02	150.0	284.0	0.64	53983	0.03	2.480	0.9	0.13363	0.4		2184	17	2146	7	-3.8	1.5
n3763-03	22.0	38.0	1.35	21187	0.09	2.587	1.0	0.13151	0.9		2107	17	2118	16	-2.4	0.7
n3763-04	211.0	382.0	1.06	605	3.09	2.622	1.0	0.13493	1.2		2083	17	2163	21	-2.1	1.6
n3763-05	150.0	282.0	0.73	94405	0.02	2.518	1.0	0.13316	0.3		2156	17	2140	6		
n3763-06	178.0	335.0	0.69	137230	0.01	2.504	1.0	0.13360	0.4		2166	18	2146	6	-3.4	1.0
n3763-07	121.0	278.0	0.54	1568	1.19	2.997	1.0	0.13082	0.5	-11.1	1856	16	2109	9	-2.3	1.5
n3763-08	82.0	150.0	0.76	12369	0.15	2.483	1.0	0.13501	0.5		2181	18	2164	9	-2.4	1.0
n3763-09	126.0	252.0	0.46	19428	0.10	2.509	1.0	0.13272	0.4		2163	17	2134	6		
n3763-10	105.0	197.0	0.77	224798	0.01	2.529	0.9	0.13201	0.4		2148	17	2125	8	-2.3	1.1
n3763-11	119.0	264.0	0.65	7863	0.24	2.974	1.0	0.13018	0.4	-10.3	1869	15	2100	7		
n3763-12	55.0	104.0	0.76	163065	0.01	2.555	0.9	0.13254	0.6		2129	17	2132	10		
n3763-13	96.0	201.0	0.55	14553	0.13	2.716	1.0	0.13155	0.5	-2.6	2021	17	2119	9		
n3763-14	129.0	268.0	0.45	1399	1.34	2.614	0.9	0.13128	0.6		2088	17	2115	11	-3.0	1.2
n3763-15	33.0	60.0	0.31	4455	0.42	2.284	1.0	0.16045	0.9	-1.8	2341	19	2460	15	-10.9	1.1
n3763-16	129.0	232.0	1.20	20980	0.09	2.665	1.0	0.13244	0.5	-1.4	2054	17	2131	8	-2.5	0.7
n3763-HF-18															-0.3	1.4
PK105																
n3690-01	58.0	109.0	0.46	97238	0.02	2.394	0.7	0.14025	0.4		2250	13	2230	6	5.9	0.9
n3690-02	124.0	278.0	0.13	12505	0.15	2.644	0.6	0.13538	0.3	-3.7	2068	11	2169	5	5.7	0.8
n3690-03	49.0	279.0	0.15	1399	1.34	7.019	0.8	0.12718	0.6	-59.3	859	6	2059	10		
n3690-04	28.0	61.0	0.23	82765	0.02	2.593	0.8	0.13667	0.5	-1.8	2103	13	2185	9	5.3	0.9
n3690-05	64.0	124.0	0.39	1572	1.19	2.432	1.0	0.13992	0.6		2220	18	2226	10	5.3	0.7
n3690-06	87.0	167.0	0.41	136012	0.01	2.415	1.0	0.13987	0.4		2233	18	2226	7		
n3690-07	127.0	252.0	0.38	39147	0.05	2.475	1.0	0.13984	0.4		2188	18	2225	7	4.5	0.7
n3690-08	130.0	243.0	0.48	92792	0.02	2.386	1.0	0.14006	0.3		2257	19	2228	6	4.6	0.8
n3690-09	220.0	499.0	0.39	33544	0.06	2.858	1.2	0.13490	0.5	-9.3	1934	20	2163	8		
n3690-10	66.0	126.0	0.47	30111	0.06	2.426	1.0	0.13935	0.5		2225	18	2219	8		
n3690-11	109.0	218.0	0.35	9036	0.21	2.483	0.9	0.13639	0.4		2181	17	2182	8	4.4	0.8
n3690-12	54.0	101.0	0.68	2803	0.67	2.514	1.0	0.13837	0.6		2159	19	2207	11	5.6	0.7
n3690-13	110.0	446.0	0.07	1630	1.15	4.719	0.9	0.12449	0.5	-39.9	1239	11	2022	9		
n3690-14	90.0	178.0	0.34	8302	0.23	2.436	1.0	0.13718	0.4		2218	18	2192	8	4.6	1.6
n3690-15	93.0	203.0	0.22	9120	0.21	2.602	1.0	0.13553	0.6	-0.7	2096	18	2171	11	5.1	0.8
n3690-16	154.0	248.0	1.83	1155	1.62	2.733	0.9	0.13603	0.7	-5.6	2010	16	2177	12		
n3690-17	59.0	119.0	0.27	189162	0.01	2.436	1.0	0.14082	0.5		2217	19	2237	9	4.8	0.8
n3690-18	93.0	178.0	0.42	100088	0.02	2.407	1.0	0.14028	0.4		2240	18	2231	7	6.3	0.7
n3690-19	203.0	638.0	0.44	1395	1.34	4.130	1.0	0.12318	0.8	-30.0	1398	12	2000			

Sample Spot #	[Pb]	[U]	Th/U	$\frac{^{206}\text{Pb}}{^{204}\text{Pb}}$	$f^{206}\text{Pb}^a$	$\frac{^{235}\text{U}}{^{238}\text{U}}$	$\pm\sigma\%$	$\frac{^{207}\text{Pb}}{^{206}\text{Pb}}$	$\pm\sigma\%$	%Disc ^b	$\frac{^{206}\text{Pb}}{^{238}\text{U}}$	$\pm\sigma$	$\frac{^{207}\text{Pb}}{^{235}\text{U}}$	$\pm\sigma$	tHF	$\pm 2\sigma$
	ppm	ppm	calc.		%					2 σ -limit	age (Ma)		age (Ma)			
ASGH003A																
n3682-01	252.0	2977.0	0.06	2998	0.62	13.220	3.8	0.07865	2.1	-45.2	470	17	1112	42	5.4	1.0
n3682-02	298.0	1212.0	0.06	11536	0.16	4.651	1.2	0.11815	0.2	-36.6	1255	13	1928	4	3.9	1.0
n3682-03	337.0	913.0	0.04	1791	1.04	3.068	1.5	0.12093	1.0	-3.5	1819	23	1970	18	2.7	1.4
n3682-04	229.0	1472.0	0.04	21671	0.09	7.202	2.5	0.09780	1.1	-44.0	838	19	1583	20	3.0	1.5
n3682-05	550.0	1725.0	0.10	4447	0.42	3.623	1.2	0.11973	0.6	-18.7	1571	17	1952	11	3.3	0.8
n3682-06	182.0	1841.0	0.00	4060	0.46	10.874	1.5	0.07174	1.6	-32.7	567	8	979	32		
n3682-07	181.0	517.0	0.06	10845	0.17	3.293	4.1	0.13046	0.6	-14.4	1709	62	2104	10	3.1	1.5
n3682-08	269.0	610.0	0.06	3827	0.49	2.606	1.2	0.13176	0.4		2093	22	2122	7	-0.2	1.7
n3682-09	753.0	1941.0	0.10	3912	0.48	2.992	1.2	0.12836	0.2	-9.8	1859	19	2076	3	2.4	1.5
n3682-10	248.0	1907.0	0.05	7311	0.26	8.654	1.5	0.09442	1.6	-47.7	705	10	1517	30	3.3	1.1
n3682-11	182.0	1889.0	0.02	12142	0.15	11.308	1.4	0.07928	0.8	-50.9	546	7	1179	15	4.1	1.3
n3682-12	218.0	2350.0	0.03	7814	0.24	11.853	2.7	0.07751	1.7	-44.7	522	13	1134	34	3.8	1.6
n3682-12b															4.0	0.8
n3682-13	265.0	588.0	0.07	63303	0.03	2.559	1.2	0.13220	0.2		2127	21	2127	4		
n3682-14	1903.0	5726.0	0.04	1863	1.00	3.436	1.2	0.12659	0.2	-20.3	1647	17	2051	3	4.3	1.4
n3682-15	251.0	579.0	0.07	10935	0.17	2.664	1.3	0.13229	0.5	-0.7	2055	24	2129	8	3.0	1.0
n3682-16	384.0	855.0	0.08	2980	0.63	2.565	1.9	0.13050	0.7		2122	34	2105	12		
n3682-17	273.0	680.0	0.08	5859	0.32	2.872	2.2	0.13060	0.2	-5.8	1926	37	2106	4	2.0	0.8
n3682-18	982.0	3298.0	0.08	2332	0.80	3.834	3.7	0.11298	2.0	-10.8	1494	49	1848	35	2.5	0.9
n3682-19	577.0	1739.0	0.05	324	5.78	3.440	1.4	0.12465	1.0	-16.4	1645	21	2024	17	2.5	0.9
n3682-20	570.0	1654.0	0.09	1142	1.64	3.362	0.9	0.12607	0.3	-18.3	1679	14	2044	5	3.1	1.0
n3682-21	241.0	1272.0	0.05	5266	0.36	6.011	1.6	0.11351	1.0	-45.2	992	14	1856	18	3.6	1.0
n3682-22	244.0	1502.0	0.03	12386	0.15	6.906	1.4	0.10512	0.6	-49.3	872	11	1716	11	3.9	1.0
ASGH007A																
n3684-01	49.0	108.0	0.34	13638	0.14	2.721	0.9	0.13634	0.6	-5.7	2018	16	2181	10	2.7	1.1
n3684-02	153.0	871.0	0.11	1013	1.85	6.809	1.1	0.11959	0.8	-54.5	883	9	1950	14		
n3684-03	48.0	118.0	0.35	17983	0.10	3.064	1.1	0.13634	0.9	-14.9	1821	17	2181	15		
n3684-04	28.0	64.0	0.31	47746	0.04	2.791	0.9	0.13610	0.8	-7.1	1974	16	2178	14	3.7	1.3
n3684-05	17.0	36.0	0.51	13837	0.14	2.849	1.0	0.13612	1.1	-7.7	1939	17	2178	19	5.2	0.9
n3684-06	41.0	88.0	0.40	49280	0.04	2.702	0.9	0.13628	0.7	-4.8	2030	16	2181	11	3.3	1.4
n3684-07	39.0	118.0	0.37	285	6.57	3.930	1.3	0.13361	5.0	-14.4	1461	17	2146	85	1.3	1.3
n3684-08	33.0	71.0	0.34	19862	0.09	2.691	1.0	0.13461	0.7	-2.9	2037	18	2159	13	3.1	0.7
n3684-09	32.0	67.0	0.49	11210	0.17	2.754	0.9	0.13685	0.8	-6.5	1997	16	2188	13	3.7	0.9
n3684-10	129.0	1291.0	0.03	328	5.70	11.767	2.7	0.13278	1.5	-71.1	526	14	2135	25		
n3684-11	51.0	118.0	0.47	3217	0.58	2.988	0.9	0.13294	0.8	-11.2	1861	15	2137	14		
n3684-12	98.0	445.0	0.30	686	2.73	6.007	0.9	0.12754	0.9	-51.5	993	8	2064	16		
n3684-Hf-13															3.2	0.7
n3684-Hf-14															2.5	0.5
ASGH022A																
n3685-01	191.0	387.0	0.50	248017	0.01	2.575	1.0	0.12901	0.3		2115	18	2085	5	4.5	1.2
n3685-02	286.0	597.0	0.55	16598	0.11	2.687	1.0	0.12925	0.2	-0.5	2040	17	2088	4	4.3	1.3
n3685-03	145.0	305.0	0.43	6919	0.27	2.639	1.0	0.12894	0.8		2071	18	2084	13		
n3685-04	359.0	697.0	0.67	36206	0.05	2.550	1.0	0.12968	0.2		2133	18	2094	4	4.9	0.9
n3685-05	125.0	264.0	0.35	33493	0.06	2.582	1.0	0.13003	0.3		2110	18	2098	5	4.8	0.8
n3685-06	200.0	391.0	0.66	28353	0.07	2.560	1.0	0.12970	0.3		2125	18	2094	5	4.7	0.9
n3685-07	47.0	101.0	0.33	42498	0.04	2.633	1.0	0.13022	0.5		2075	18	2101	9		
n3685-08	572.0	1273.0	0.07	588018	0.00	2.556	1.0	0.12979	0.1		2129	19	2095	2	3.4	1.5
n3685-09	122.0	263.0	0.38	16537	0.11	2.670	1.0	0.12924	0.4		2051	17	2088	6	3.9	1.5
n3685-10	368.0	846.0	0.09	36268	0.05	2.660	1.0	0.12975	0.2	0.0	2057	18	2095	3	4.3	1.2
n3685-11	293.0	596.0	0.56	265949	0.01	2.621	1.0	0.12968	0.2		2083	17	2094	4	3.9	0.8
ASGH022C																
n3686-01	211.0	447.0	0.43	21933	0.09	2.654	1.1	0.12951	0.2		2062	19	2091	4	5.5	1.3
n3686-02	166.0	367.0	0.38	1066	1.75	2.744	1.0	0.13042	1.0	-0.9	2003	18	2104	17	3.7	1.4
n3686-03	109.0	239.0	0.25	566	3.30	2.623	1.0	0.12831	0.6		2082	18	2075	11	4.9	0.6
n3686-04	216.0	480.0	0.25	4235	0.44	2.670	1.0	0.12962	0.3	-0.1	2051	17	2093	5	3.8	0.9
n3686-05	143.0	314.0	0.34	1985	0.94	2.684	1.0	0.12892	0.4	-0.2	2035	17	2083	7	4.3	0.7
n3686-06	172.0	380.0	0.27	17615	0.11	2.664	1.0	0.13008	0.3	-0.3	2055	17	2099	4	3.2	0.7
n3686-07	112.0	242.0	0.30	12111	0.15	2.618	1.0	0.12950	0.4		2085	17	2091	7	4.2	0.9

^aWhere the letter b is added to spot name it indicates a second spot in an already analysed grain.

^b% of common ²⁰⁶Pb in measured ²⁰⁶Pb, estimated from ²⁰⁴Pb assuming a present day Stacey and Kramers (1975) model for terrestrial Pb-isotope composition.

^cAge discordance at closest approach of error ellipse to concordia (2 σ level).

Italic denote discarded analyses not used in calculations.

Table 2. Lu-Hf

Grain#	¹⁷⁶ Hf ¹⁷⁷ Hf	2SE	¹⁷⁶ Lu ¹⁷⁷ Hf	2SE	¹⁷⁶ Yb ¹⁷⁷ Hf	¹⁷⁶ Hf ¹⁷⁷ Hf	2SE	Assigned age (Ma)	±s	¹⁷⁶ Hf ¹⁷⁷ Hf _i	±Hf	±2σ	ΔεHf	Hf _{DM} [*] (Ma)
	2SD outlier rejection	×E-6	no outlier rejection	×E-5			×E-5							
PK101														
n3762-Hf-05	0.2813382	19	0.0007683	2	0.0212	1.46728	6	2126	12	0.2813071	-4.17	0.69	1.1	2688
n3762-Hf-06	0.2813663	20	0.0005982	1	0.0169	1.46728	8	2126	12	0.2813424	-2.92	0.71	0.8	2625
n3762-Hf-07	0.2814046	46	0.0009564	6	0.0204	1.46731	14	2126	12	0.2813765	-1.71	1.62	1.0	2564
n3762-Hf-09	0.2814158	39	0.0007041	1	0.0194	1.46730	10	2126	12	0.2813873	-1.32	1.4	1.0	2545
n3762-Hf-10	0.2814186	39	0.0008826	2	0.0250	1.46727	9	2126	12	0.2813829	-1.48	1.4	1.3	
n3762-Hf-12	0.2813620	44	0.0006292	2	0.0160	1.46732	7	2126	12	0.2813366	-3.13	1.5	0.9	2635
n3762-Hf-13	0.2813785	16	0.0006319	1	0.0163	1.46729	3	2126	12	0.2813529	-2.54	0.6	0.9	2606
n3762-Hf-14	0.2813544	16	0.0006185	1	0.0172	1.46729	3	2126	12	0.2813293	-3.38	0.6	0.9	2648
n3762-Hf-15	0.2813700	18	0.0006245	4	0.0159	1.46730	4	2126	12	0.2813448	-2.83	0.7	0.9	2621
PK102														
n3689-Hf-1	0.2815510	179	0.0018695	18	0.0516	1.46747	14	2174	6	0.2814735	2.9	1.6	2.8	2375
n3688-Hf-2	0.2815102	77	0.0011261	8	0.0291	1.46722	7	2174	6	0.2814636	2.5	0.9	1.7	2393
n3688-Hf-3a	0.2814538	79	0.0005755	8	0.0143	1.46729	7	2174	6	0.2814299	1.3	0.7	0.8	2453
n3688-Hf-3b	0.2814848	66	0.0009240	7	0.0240	1.46721	5	2174	6	0.2814465	1.9	0.5	1.4	2424
n3688-Hf-4	0.2815630	109	0.0022778	11	0.0655	1.46728	8	2174	6	0.2814686	2.7	1.1	3.4	2384
n3688-Hf-5	0.2815392	29	0.0011070	3	0.0262	1.46725	7	2174	6	0.2814844	3.2	0.6	1.6	2356
n3688-Hf-6	0.2815326	65	0.0014255	6	0.0373	1.46726	6	2174	6	0.2814735	2.9	1.1	2.1	2375
n3688-Hf-7	0.2814986	24	0.0012834	2	0.0324	1.46726	6	2174	6	0.2814454	1.9	0.5	1.9	2426
n3688-Hf-8	0.2814972	64	0.0020388	6	0.0572	1.46727	12	2174	6	0.2814127	0.7	1.4	3.0	2484
n3688-Hf-9	0.2814772	108	0.0011156	11	0.0307	1.46737	12	2174	6	0.2814310	1.3	1.3	1.6	2452
n3688-Hf-10	0.2815902	58	0.0012214	6	0.0310	1.46724	11	2174	6	0.2815396	5.2	0.9	1.8	2257
n3688-Hf-11	0.2815020	41	0.0013264	4	0.0334	1.46726	9	2174	6	0.2814471	1.9	0.9	2.0	2423
n3688-Hf-13	0.2814588	38	0.0007033	4	0.0188	1.46724	7	2174	6	0.2814296	1.3	0.8	1.0	2454
n3688-Hf-14	0.2815216	30	0.0012601	3	0.0333	1.46731	6	2174	6	0.2814697	2.7	0.7	1.9	2382
n3688-Hf-15	0.2815158	44	0.0009915	4	0.0269	1.46727	6	2174	6	0.2814747	2.9	0.7	1.5	2373
n3688-Hf-16	0.2815337	93	0.0014410	9	0.0402	1.46725	7	2174	6	0.2814740	2.9	0.9	2.1	2375
n3688-Hf-17	0.2815563	74	0.0015507	7	0.0413	1.46714	5	2174	6	0.2814921	3.5	0.6	2.3	2342
n3688-Hf-18	0.2814859	25	0.0015899	3	0.0407	1.46729	5	2174	6	0.2814201	1.0	0.8	2.3	2471
n3689-Hf-19	0.2815158	40	0.0012900	4	0.0329	1.46727	3	2174	6	0.2814624	2.5	0.5	1.9	2395
PK103														
n3763-Hf-1	0.2815158	0	0.0012900	4	0.0329	1.46727	3	2139	5	0.2814633	1.7	0.5	1.9	2405
n3763-Hf-2	0.2813399	41	0.0007544	6	0.0228	1.46720	11	2139	5	0.2813091	-3.8	1.5	1.1	2690
n3763-Hf-3	0.2813968	18	0.0012151	7	0.0347	1.46733	6	2139	5	0.2813473	-2.4	0.7	1.8	2612
n3763-Hf-4	0.2813798	44	0.0005659	5	0.0170	1.46734	13	2139	5	0.2813567	-2.1	1.6	0.8	2595
n3763-Hf-6	0.2813449	29	0.0006590	5	0.0194	1.46722	10	2139	5	0.2813180	-3.5	1.0	1.0	2664
n3763-Hf-7	0.2813862	42	0.0008793	4	0.0243	1.46715	11	2139	5	0.2813503	-2.3	1.5	1.3	2607
n3763-Hf-8	0.2813820	28	0.0006243	4	0.0244	1.46718	7	2139	5	0.2813484	-2.4	1.0	1.2	2610
n3763-Hf-10	0.2813763	32	0.0006892	1	0.0188	1.46733	10	2139	5	0.2813502	-2.9	1.1	1.0	2607
n3763-Hf-13a	0.2812941	21	0.0009154	3	0.0236	1.46720	9	2139	5	0.2812468	-6.0	0.7	1.3	
n3763-Hf-13b	0.2813413	29	0.0011983	6	0.0308	1.46712	16	2139	5	0.2812925	-4.4	1.0	1.7	
n3763-Hf-14	0.2813507	34	0.0005279	1	0.0140	1.46712	11	2139	5	0.2813292	-3.1	1.2	0.8	2644
n3763-Hf-15	0.2811160	30	0.0001662	1	0.0044	1.46723	10	2139	5	0.2811092	-10.9	1.1	0.2	
n3763-Hf-16	0.2813822	19	0.0009072	5	0.0253	1.46720	7	2139	5	0.2813453	-2.5	0.7	1.3	2616
n3763-Hf-18	0.2814713	38	0.0015994	12	0.0479	1.46725	14	2139	5	0.2814061	-0.4	1.4	2.3	2507
PK105														
n3690-Hf-01	0.2815879	25	0.0015896	15	0.0401	1.46722	3	2229	4	0.2815204	5.8	0.9	2.4	2274
n3690-Hf-02	0.2815861	22	0.0016679	13	0.0433	1.46726	4	2229	4	0.2815153	5.6	0.8	2.5	2283
n3690-Hf-04	0.2815675	24	0.0014901	7	0.0387	1.46725	4	2229	4	0.2815042	5.2	0.9	2.3	2303
n3690-Hf-05	0.2815758	21	0.0018609	8	0.0421	1.46724	4	2229	4	0.2815043	5.2	0.7	2.5	2303
n3690-Hf-06	0.2815116	46	0.0023242	26	0.0618	1.46725	6	2229	4	0.2814128	2.0	1.7	3.5	2466
n3690-Hf-07	0.2815724	20	0.0021093	5	0.0537	1.46725	4	2229	4	0.2814628	4.5	0.7	3.2	2341
n3690-Hf-08	0.2815742	22	0.0020743	10	0.0526	1.46728	4	2229	4	0.2814860	4.6	0.8	3.1	2335
n3690-Hf-09	0.2815747	50	0.0018196	25	0.0479	1.46735	10	2229	4	0.2814973	5.0	1.8	2.7	
n3690-Hf-10	0.2815960	52	0.0025488	9	0.0665	1.46735	8	2229	4	0.2814877	4.6	1.9	3.9	
n3690-Hf-11	0.2815379	23	0.0013634	4	0.0340	1.46724	3	2229	4	0.2814799	4.4	0.8	2.1	2346
n3690-Hf-12	0.2815520	19	0.0009391	8	0.0236	1.46726	4	2229	4	0.2815121	5.5	0.7	1.4	2289
n3690-Hf-14	0.2816150	44	0.0030921	4	0.0794	1.46723	5	2229	4	0.2814836	4.5	1.6	4.7	2340
n3690-Hf-15	0.2815487	22	0.0012250	5	0.0320	1.46730	4	2229	4	0.2814977	5.0	0.8	1.9	2314
n3690-Hf-16	0.2815394	24	0.0010195	14	0.0251	1.46727	6	2229	4	0.2814981	4.9	0.9	1.5	2317
n3690-Hf-17	0.2815442	22	0.0012530	4	0.0318	1.46724	4	2229	4	0.2814909	4.8	0.8	1.9	2327
n3690-Hf-18	0.2816174	20	0.0019764	10	0.0514	1.46723	4	2229	4	0.2815334	6.3	0.7	3.0	2250
n3690-Hf-19a	0.2815850	42	0.0012859	6	0.0335	1.46729	7	2229	4	0.2815304	6.2	1.5	1.9	2256
n3690-Hf-19b	0.2815832	44	0.0016664	14	0.0426	1.46727	6	2229	4	0.2815124	5.5	1.6	2.5	2288
n3690-Hf-20a	0.2816103	46	0.0021971	25	0.0571	1.46721	6	2229	4	0.2815169	5.7	1.7	3.3	2280
n3690-Hf-20b	0.2815996	56	0.0022827	22	0.0597	1.46727	7	2229	4	0.2815026	5.2	2.0	3.4	2306
n3690-Hf-21	0.2815939	23	0.0021463	6	0.0535	1.46728	5	2229	4	0.2815029	5.2	0.8	3.2	2305
n3690-Hf-22	0.2816455	26	0.0028531	18	0.0741	1.46725	4	2229	4	0.2815242	5.9	1.0	4.3	2267
n3690-Hf-23	0.2815936	28	0.0020816	11	0.0541	1.46728	4	2229	4	0.2815051	5.3	1.0	3.1	2301
n3690-Hf-24	0.2815402	24	0.0012179	11	0.0319	1.46726	4	2229	4	0.2814884	4.7	0.9	1.8	2331
n3690-Hf-27	0.2815537	26	0.0015787	15	0.0410	1.46726	4	2229	4	0.2814866	4.6	1.0	2.4	2334
n3690-Hf-28	0.2815438	27	0.0015463	7	0.0413	1.46725	5	2229	4	0.2814781	4.3	1.0	2.3	2349
n3690-Hf-29	0.2815757	39	0.0026346	8	0.0697	1.46724	7	2229	4	0.2814637	3.8	1.4	4.0	2375
n3690-Hf-30	0.2815563	17	0.0014079	7	0.0349	1.46725	5	2229	4	0.2814965	4.9	0.6	2.1	2317
n3690-Hf-31	0.2815933	24	0.0021192	7	0.0560	1.46723	5	2229	4	0.2815033	5.2	0.8	3.2	2304
n3690-Hf-32	0.2814988	35	0.0013306	7	0.0346	1.46726	6	2229	4	0.2814423	3.0	1.2	2.0	2414

Grain#	$\frac{^{176}\text{Lu}}{^{177}\text{Hf}}$	2SE	$\frac{^{176}\text{Lu}}{^{177}\text{Hf}}$	2SE	$\frac{^{176}\text{Yb}}{^{177}\text{Hf}}$	$\frac{^{176}\text{Hf}}{^{177}\text{Hf}}$	2SE	Assigned age (Ma)	±s	$\frac{^{176}\text{Lu}}{^{177}\text{Hf}}$	±Hf	±2σ	ΔtHf	Hf _{cm} (Ma)
	2SD outlier rejection	×E-6	no outlier rejection	×E-5			×E-5							
ASGH003A														
n3682-Hf-01a	0.2816195	29	0.0010369	2	0.0347	1.46723	5	2125	18	0.2815775	5.4	1.0	1.5	2205
n3682-Hf-01b	0.2817005	33	0.0013549	4	0.0448	1.46726	6	2125	18	0.2816456	7.8	1.2	1.9	2282
n3682-Hf-02	0.2815675	27	0.0008103	2	0.0259	1.46728	5	2125	18	0.2815347	3.9	1.0	1.2	2282
n3682-Hf-03	0.2815260	40	0.0005837	1	0.0181	1.46727	6	2125	18	0.2815024	2.7	1.4	0.8	2340
n3682-Hf-04	0.2815332	42	0.0006015	1	0.0178	1.46729	6	2125	18	0.2815089	3.0	1.5	0.9	2328
n3682-Hf-05	0.2815528	23	0.0008575	4	0.0288	1.46728	4	2125	18	0.2815181	3.3	0.8	1.2	2312
n3682-Hf-06	0.2815343	61	0.0011095	13	0.0320	1.46738	10	2125	18	0.2814894	2.3	2.2	1.6	
n3682-Hf-07	0.2815506	43	0.0009251	9	0.0267	1.46729	6	2125	18	0.2815132	3.1	1.5	1.3	2320
n3682-Hf-08	0.2814471	48	0.0006355	3	0.0179	1.46726	7	2125	18	0.2814214	-0.1	1.7	0.9	2484
n3682-Hf-09	0.2815156	43	0.0005744	1	0.0183	1.46730	6	2125	18	0.2814923	2.4	1.5	0.8	2358
n3682-Hf-10	0.2815804	31	0.0015164	4	0.0489	1.46728	5	2125	18	0.2815190	3.3	1.1	2.2	2310
n3682-Hf-11	0.2815775	37	0.0009299	1	0.0291	1.46726	6	2125	18	0.2815398	4.1	1.3	1.3	2273
n3682-Hf-12a	0.2815887	45	0.0013799	6	0.0468	1.46731	8	2125	18	0.2815329	3.8	1.6	2.0	2285
n3682-Hf-12b	0.2815791	23	0.0010065	1	0.0328	1.46728	5	2125	18	0.2815383	4.0	0.8	1.4	2275
n3682-Hf-13	0.2815363	32	0.0005213	1	0.0153	1.46726	6	2125	18	0.2815152	3.2	1.1	0.7	
n3682-Hf-14	0.2815796	39	0.0008272	1	0.0245	1.46730	6	2125	18	0.2815481	4.3	1.4	1.2	2281
n3682-Hf-15	0.2815583	27	0.0011916	8	0.0380	1.46731	6	2125	18	0.2815101	3.0	1.0	1.7	2326
n3682-Hf-17	0.2815072	24	0.0005928	3	0.0186	1.46728	4	2125	18	0.2814832	2.1	0.8	0.9	2374
n3682-Hf-18	0.2815251	25	0.0007090	1	0.0230	1.46725	5	2125	18	0.2814964	2.5	0.9	1.0	2350
n3682-Hf-19	0.2815251	25	0.0007090	1	0.0303	1.46735	7	2125	18	0.2814964	2.5	0.9	1.0	2350
n3682-Hf-20	0.2815574	27	0.0010641	1	0.0328	1.46729	5	2125	18	0.2815143	3.2	1.0	1.5	2318
n3682-Hf-21	0.2815605	27	0.0008508	3	0.0256	1.46725	5	2125	18	0.2815260	3.6	1.0	1.2	2297
n3682-Hf-22	0.2815692	27	0.0008444	2	0.0277	1.46725	5	2125	18	0.2815350	3.9	1.0	1.2	2281
ASGH007A														
n3684-Hf-01	0.2814912	62	0.0005408	5	0.0136	1.46729	13	2173	12	0.2814688	2.7	1.1	0.8	2384
n3684-Hf-04	0.2815246	72	0.0006500	6	0.0169	1.46723	4	2173	12	0.2814977	3.7	1.3	1.0	2333
n3684-Hf-05	0.2815730	48	0.0008127	14	0.0234	1.46724	8	2173	12	0.2815393	5.2	0.9	1.2	2258
n3684-Hf-06	0.2815151	79	0.0006882	3	0.0163	1.46726	12	2173	12	0.2814874	3.3	1.4	1.0	2351
n3684-Hf-07	0.2814489	74	0.0004333	7	0.0104	1.46745	8	2173	12	0.2814310	1.3	1.3	0.6	2452
n3684-Hf-08	0.2815035	40	0.0005311	2	0.0129	1.46726	6	2173	12	0.2814815	3.1	0.7	0.8	2362
n3684-Hf-09	0.2815233	51	0.0009472	6	0.0168	1.46721	10	2173	12	0.2814965	3.6	0.9	1.0	2335
n3684-Hf-13	0.2815108	42	0.0006857	3	0.0165	1.46728	8	2173	12	0.2814824	3.1	0.7	1.0	2380
n3684-Hf-14	0.2814911	29	0.0006315	2	0.0150	1.46721	7	2173	12	0.2814650	2.5	0.5	0.9	2391
ASGH022A														
n3685-Hf-01	0.2815723	35	0.0000316	2	0.0014	1.46726	6	2093	2	0.2815710	4.4	1.2	0.0	2227
n3685-Hf-02	0.2815675	37	0.0000379	6	0.0017	1.46729	7	2093	2	0.2815660	4.3	1.3	0.1	2236
n3685-Hf-04	0.2815847	25	0.0000434	2	0.0018	1.46725	7	2093	2	0.2815830	4.9	0.9	0.1	2206
n3685-Hf-05	0.2815868	22	0.0001742	5	0.0060	1.46729	4	2093	2	0.2815798	4.8	0.8	0.2	2211
n3685-Hf-06	0.2815833	25	0.0001117	8	0.0041	1.46721	4	2093	2	0.2815789	4.7	0.9	0.2	2213
n3685-Hf-08	0.2815511	42	0.0002567	14	0.0083	1.46725	7	2093	2	0.2815409	3.4	1.5	0.4	2281
n3685-Hf-09	0.2815578	41	0.0000561	4	0.0018	1.46721	9	2093	2	0.2815556	3.9	1.5	0.1	2255
n3685-Hf-10	0.2815719	35	0.0001131	6	0.0042	1.46730	8	2093	2	0.2815674	4.3	1.2	0.2	2234
n3685-Hf-11	0.2815613	24	0.0001342	10	0.0045	1.46730	4	2093	2	0.2815559	3.9	0.8	0.2	2254
ASGH022C														
n3686-Hf-01	0.2816063	37	0.0001513	1	0.0050	1.46732	5	2092	4	0.2816003	5.5	1.3	0.2	2175
n3686-Hf-02	0.2815582	40	0.0001863	2	0.0064	1.46729	7	2092	4	0.2815508	3.7	1.4	0.3	2264
n3686-Hf-03	0.2815878	18	0.0000713	1	0.0026	1.46729	4	2092	4	0.2815850	4.9	0.6	0.1	2292
n3686-Hf-04	0.2815579	25	0.0000892	0	0.0030	1.46724	6	2092	4	0.2815544	3.8	0.9	0.1	2257
n3686-Hf-05	0.2815747	20	0.0001714	1	0.0052	1.46728	4	2092	4	0.2815678	4.3	0.7	0.2	2233
n3686-Hf-06	0.2815474	18	0.0002945	0	0.0095	1.46728	4	2092	4	0.2815356	3.2	0.7	0.4	2291
n3686-Hf-07	0.2815704	24	0.0001399	0	0.0044	1.46727	4	2092	4	0.2815648	4.2	0.9	0.2	2238

*Two stage model ages using the measured $^{176}\text{Lu}/^{177}\text{Hf}$ of each individual analysis and the age of the zircon for the first stage, and a $^{176}\text{Lu}/^{177}\text{Hf}$ value of 0.0093 and the depleted mantle (new crust curve) reference values

$^{176}\text{Lu}/^{177}\text{Hf}$: 0.03795; $^{176}\text{Hf}/^{177}\text{Hf}$: 0.285158 of Dhruv et al. (2012) for the second stage.

Present day value of CHUR $^{176}\text{Lu}/^{177}\text{Hf}$ = 0.282785

Present day value of CHUR $^{176}\text{Lu}/^{177}\text{Hf}$ = 0.0336

$\lambda = 1.867\text{E}-11$

Italics denote where the zircon grain has been ablated through, and data is discarded.

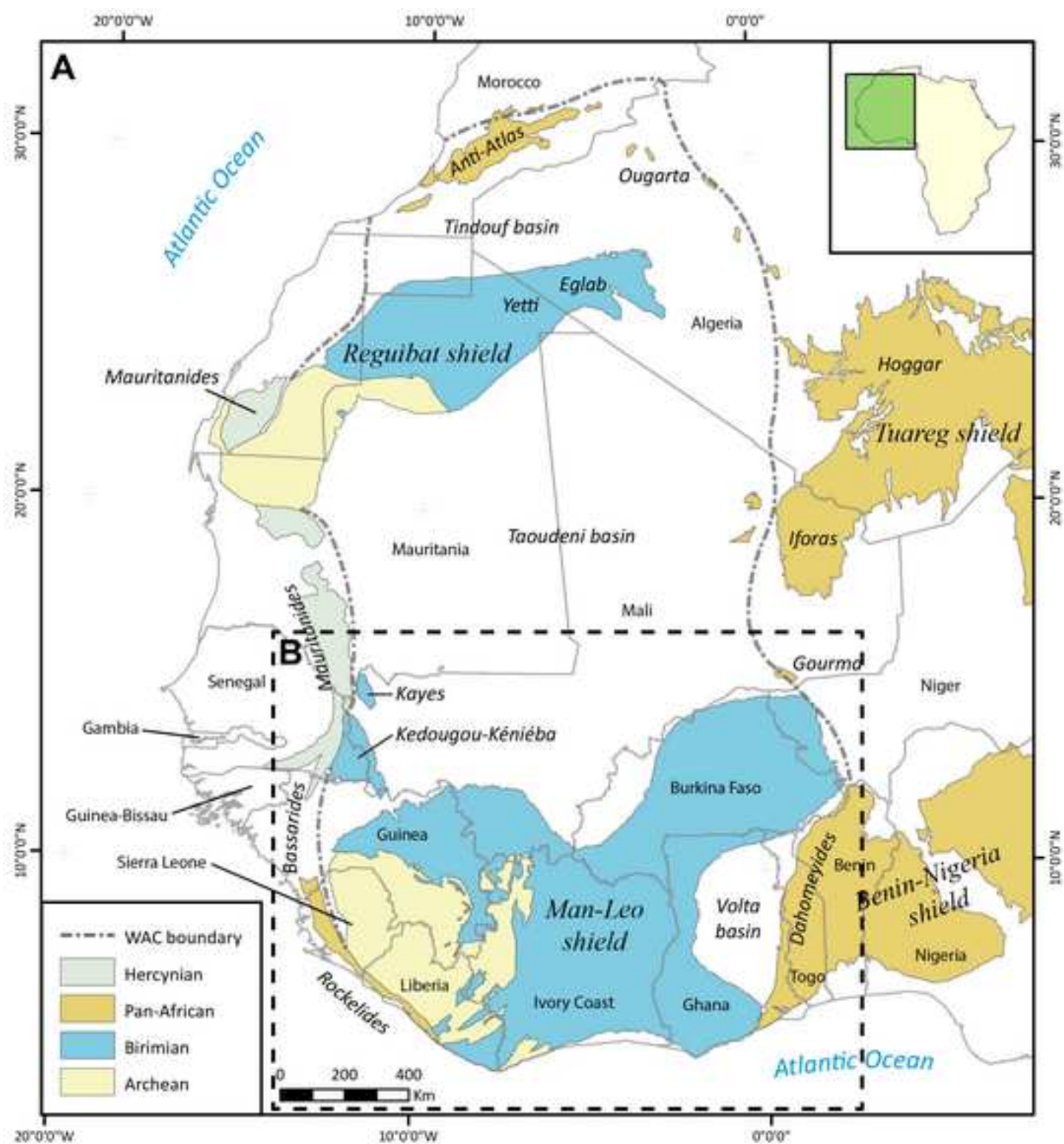
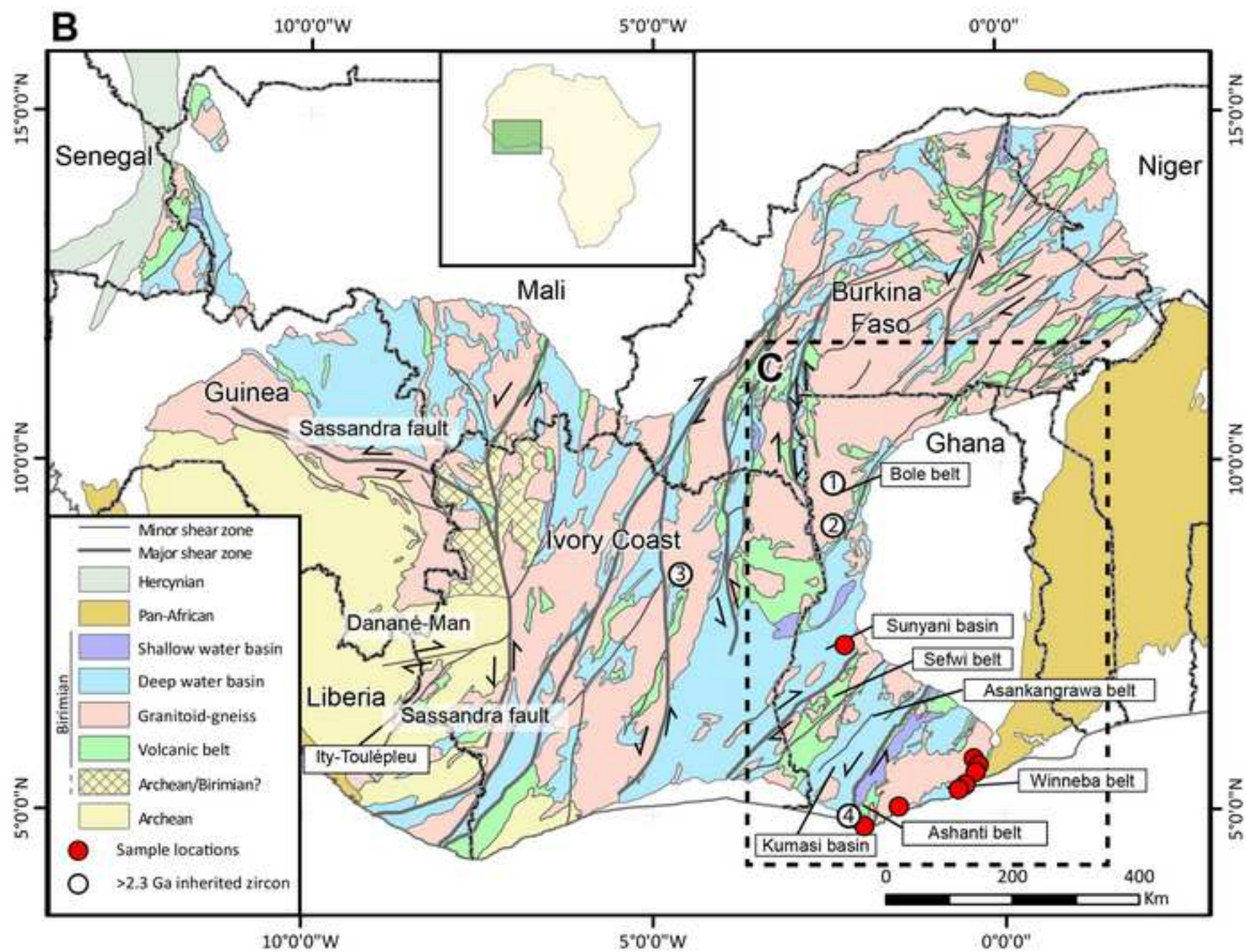
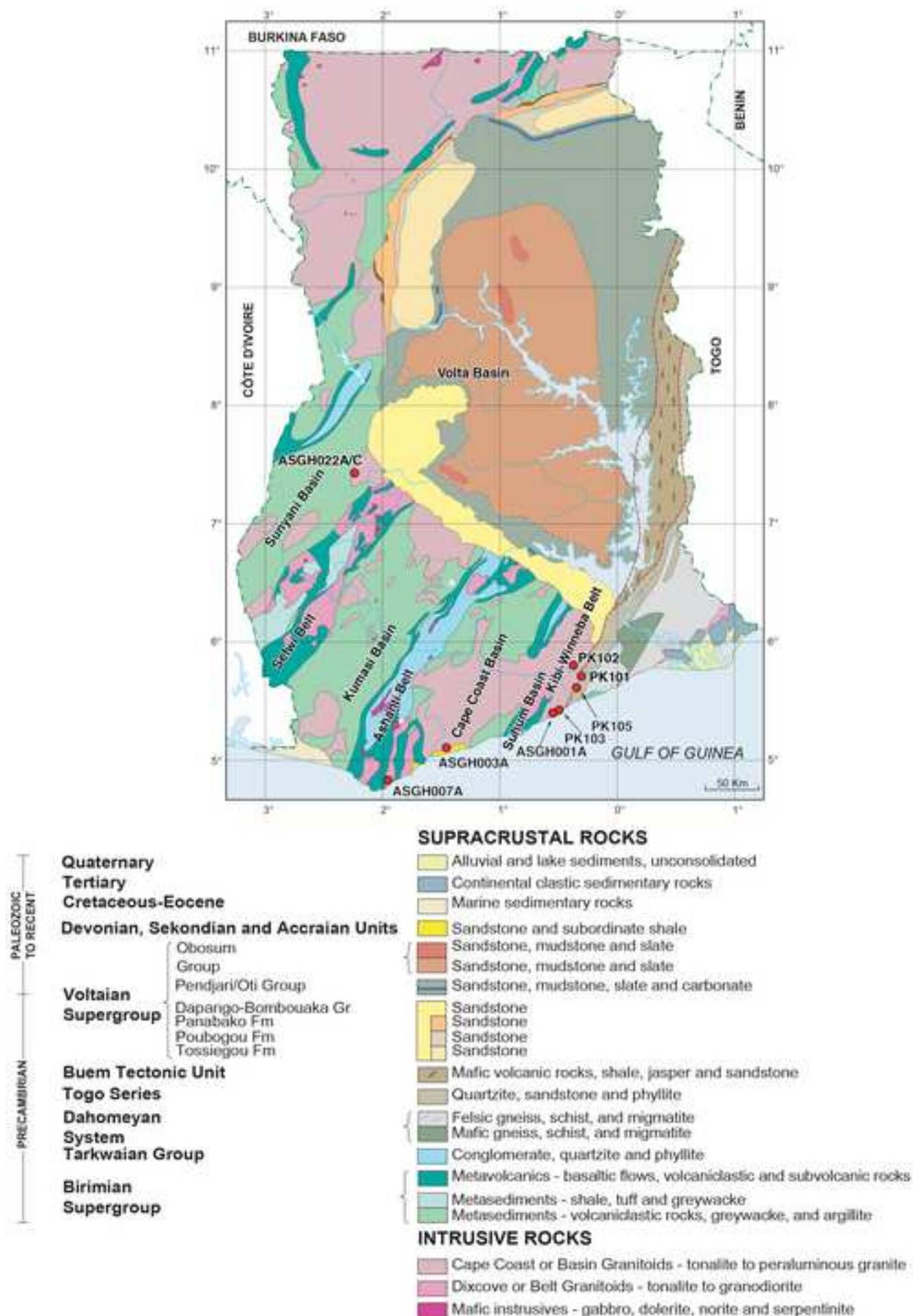
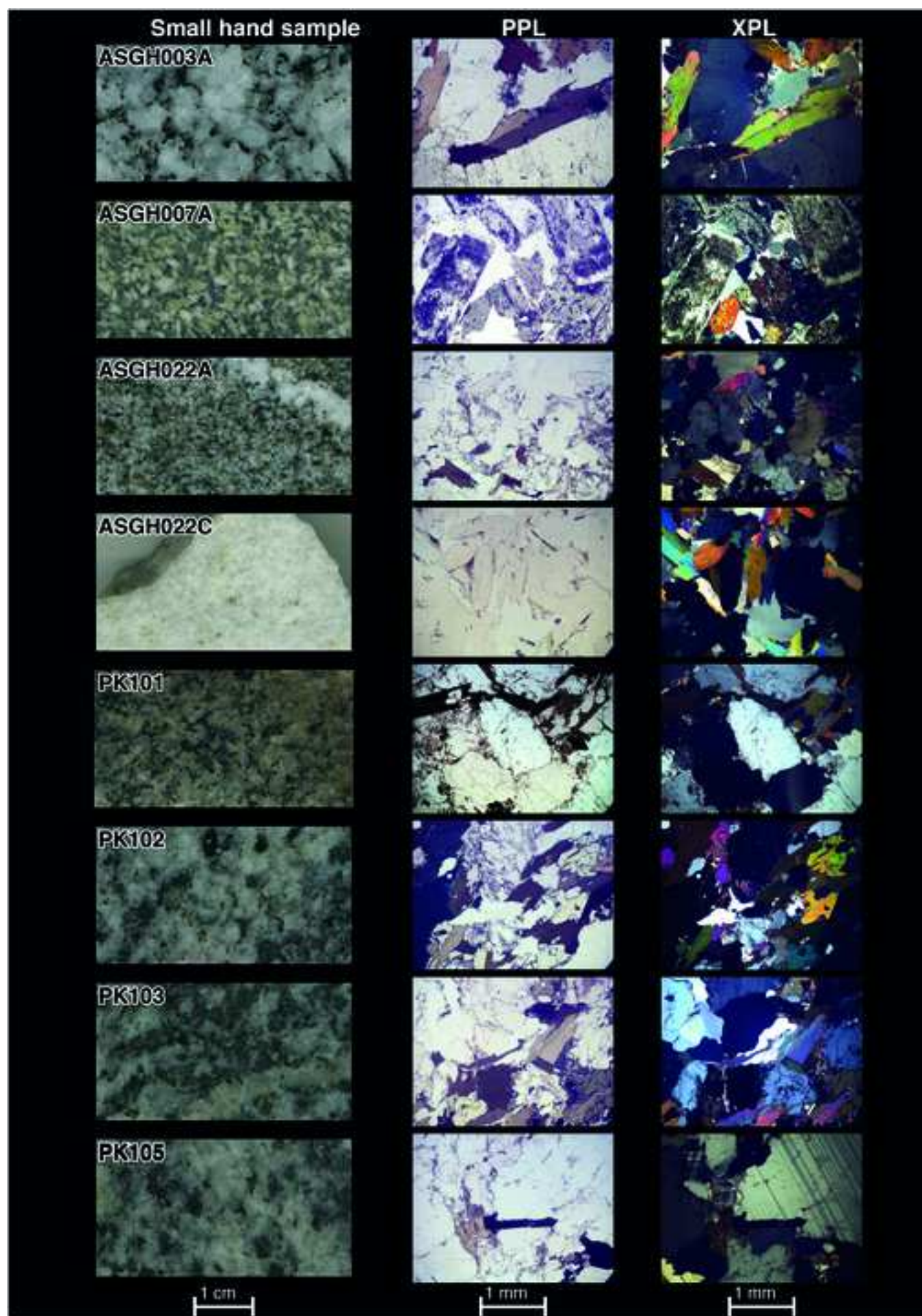


Figure 1b







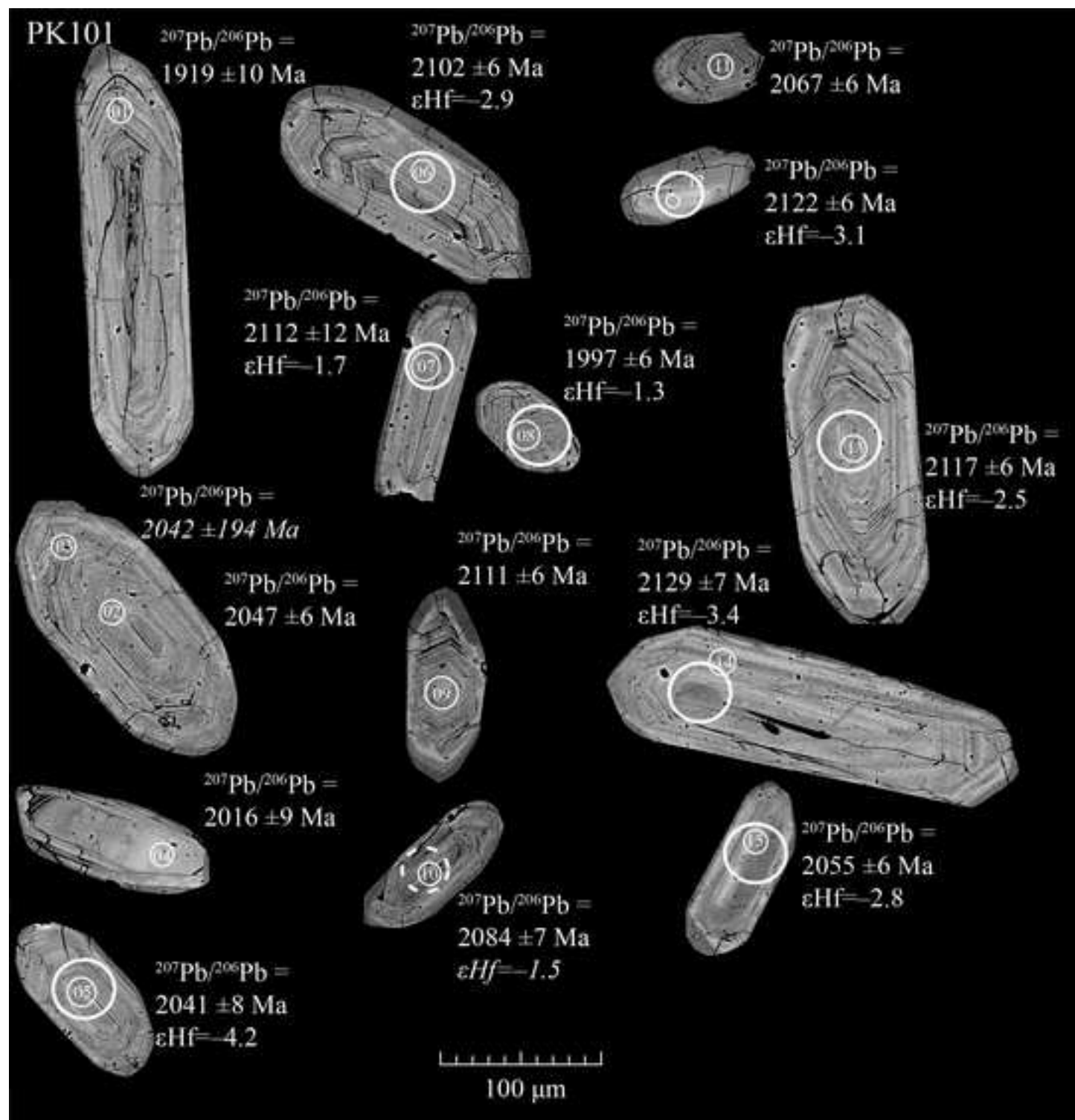


Figure 4

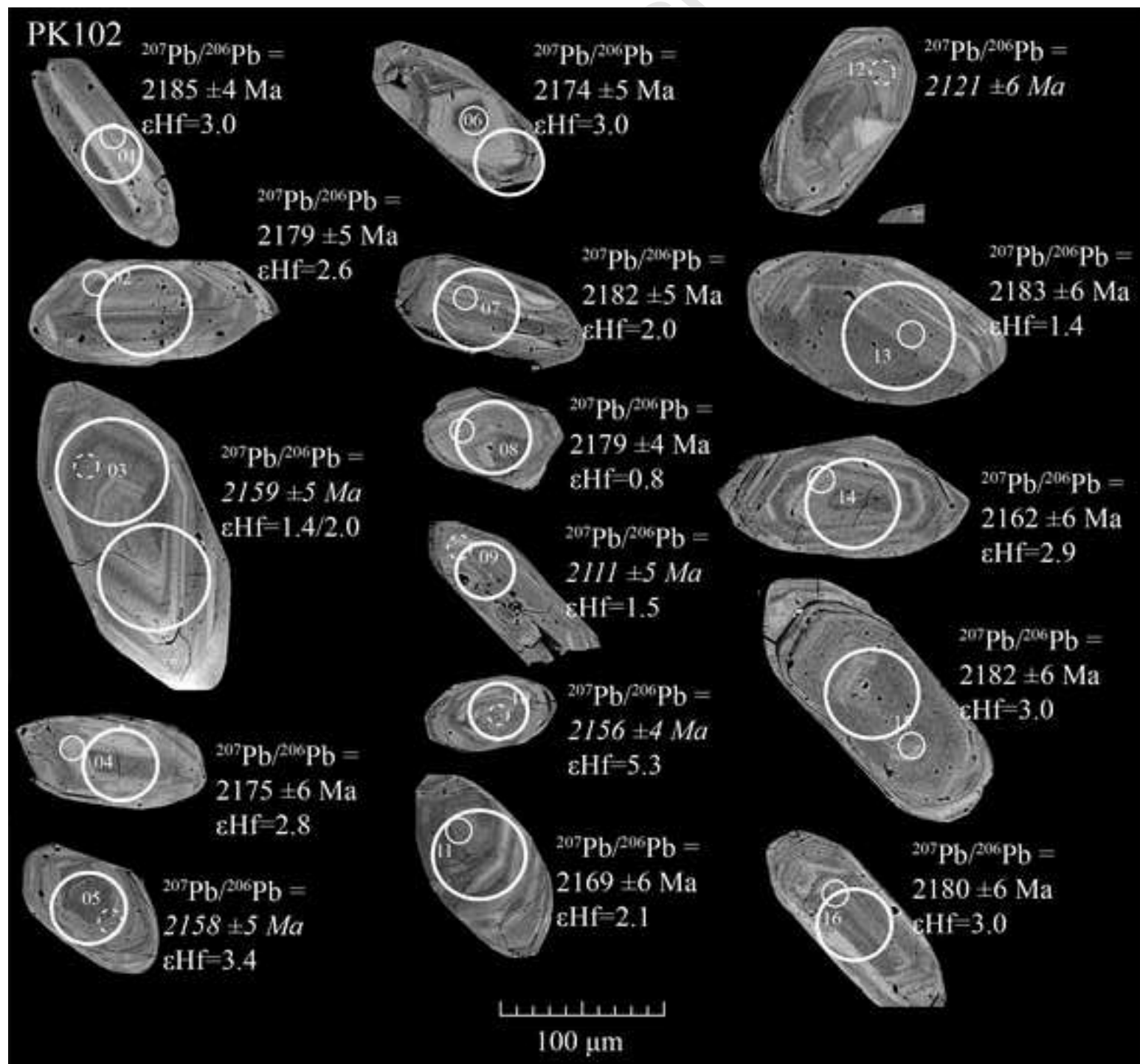


Figure 5

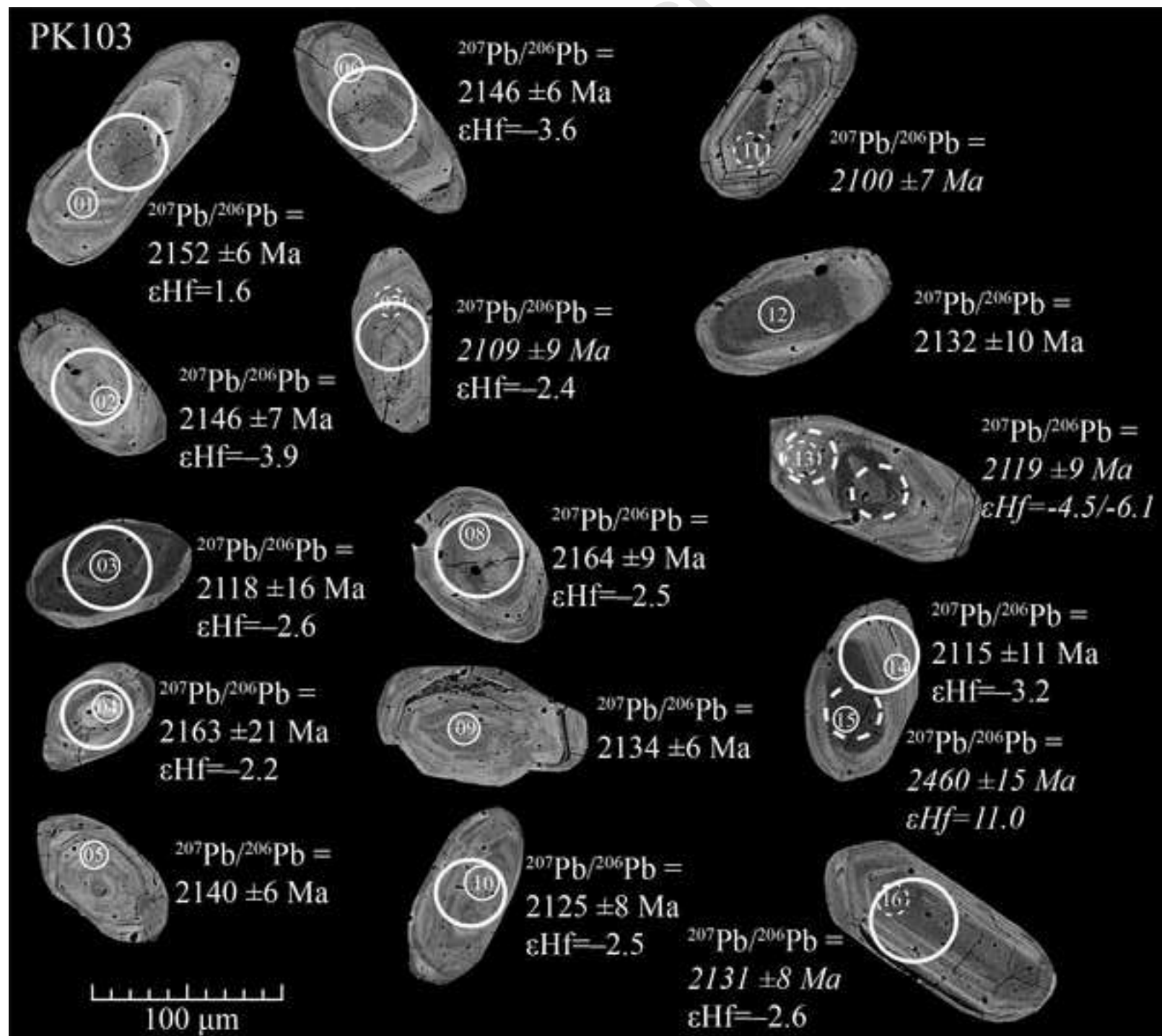
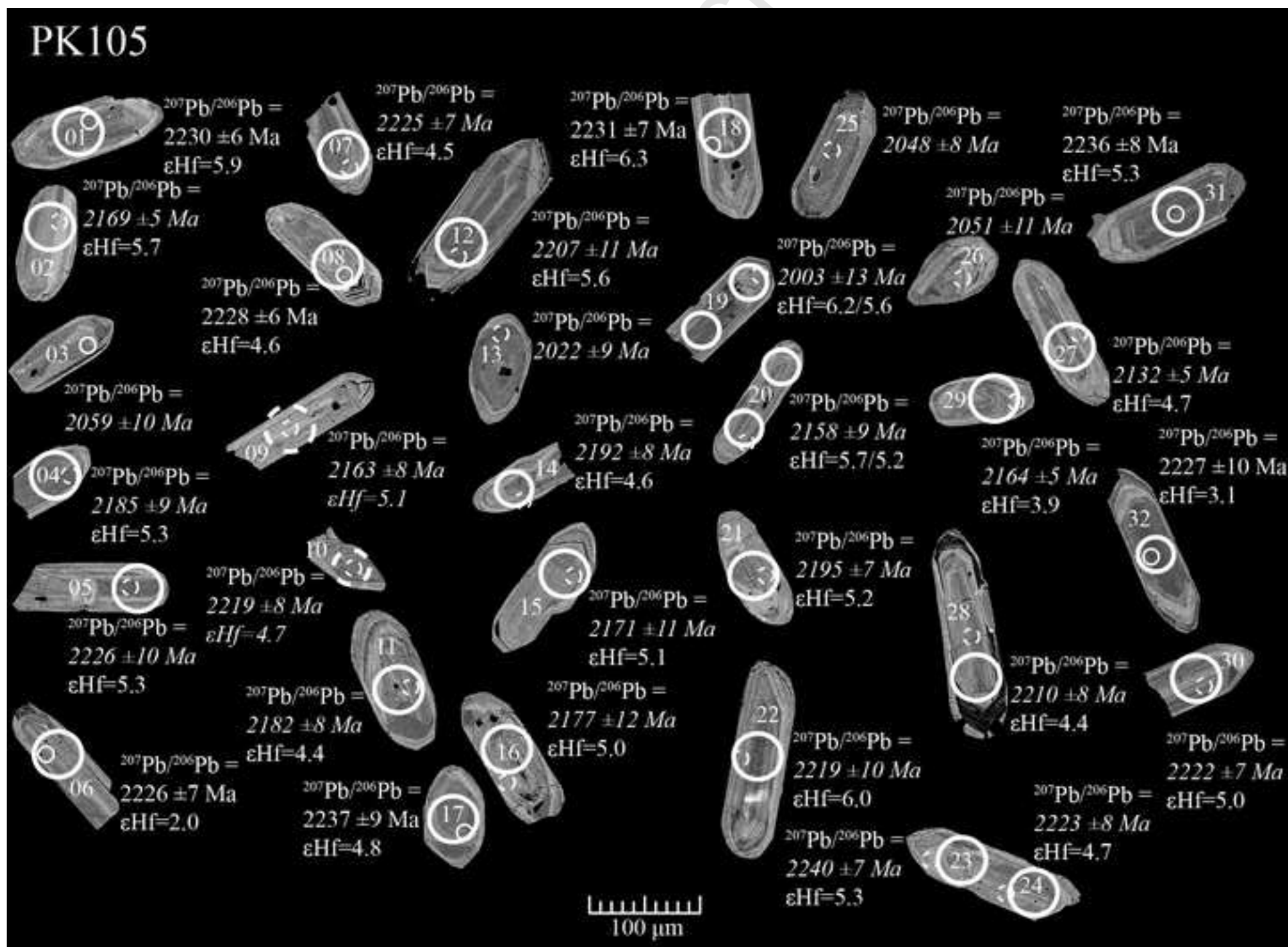


Figure 6



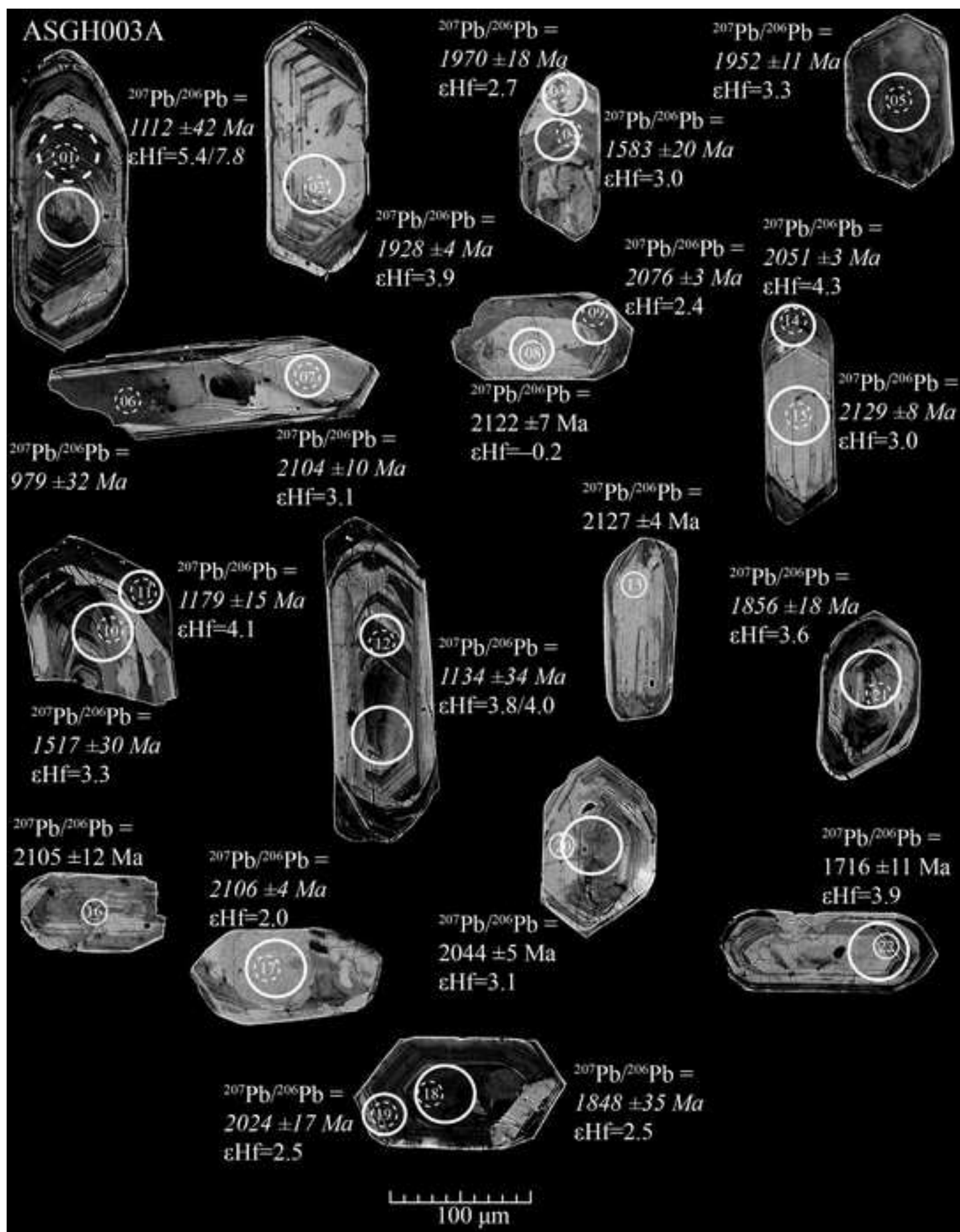


Figure 8

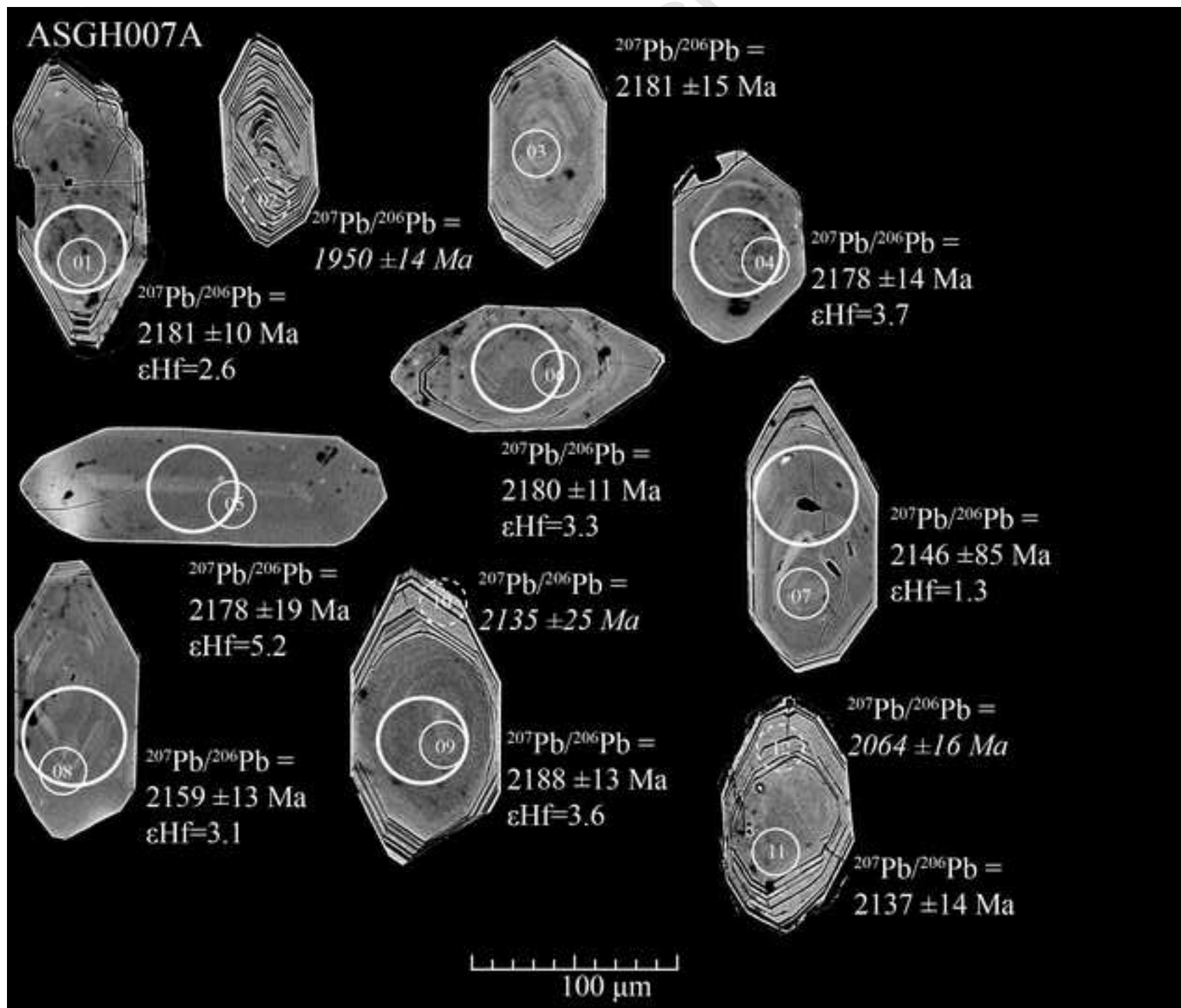
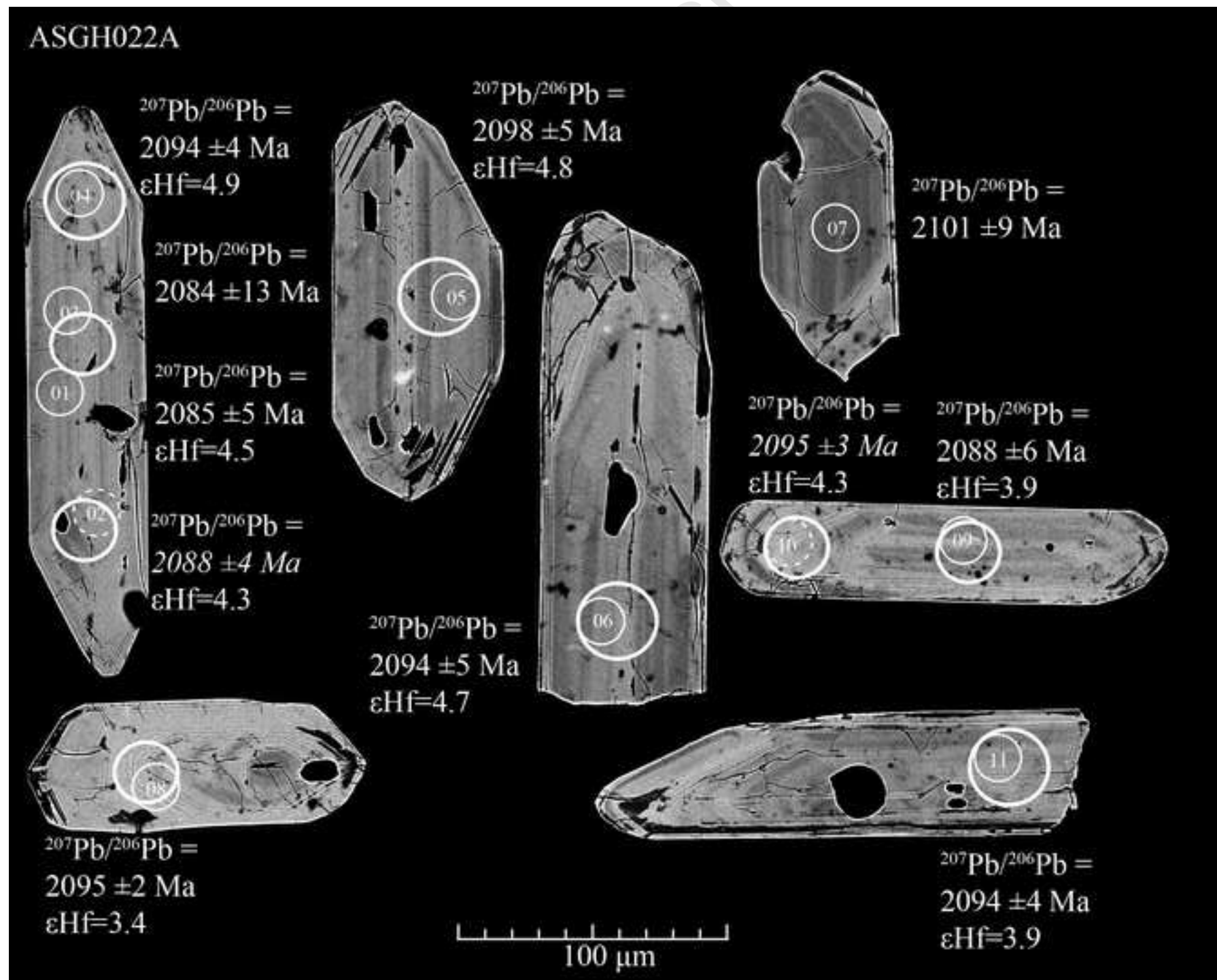
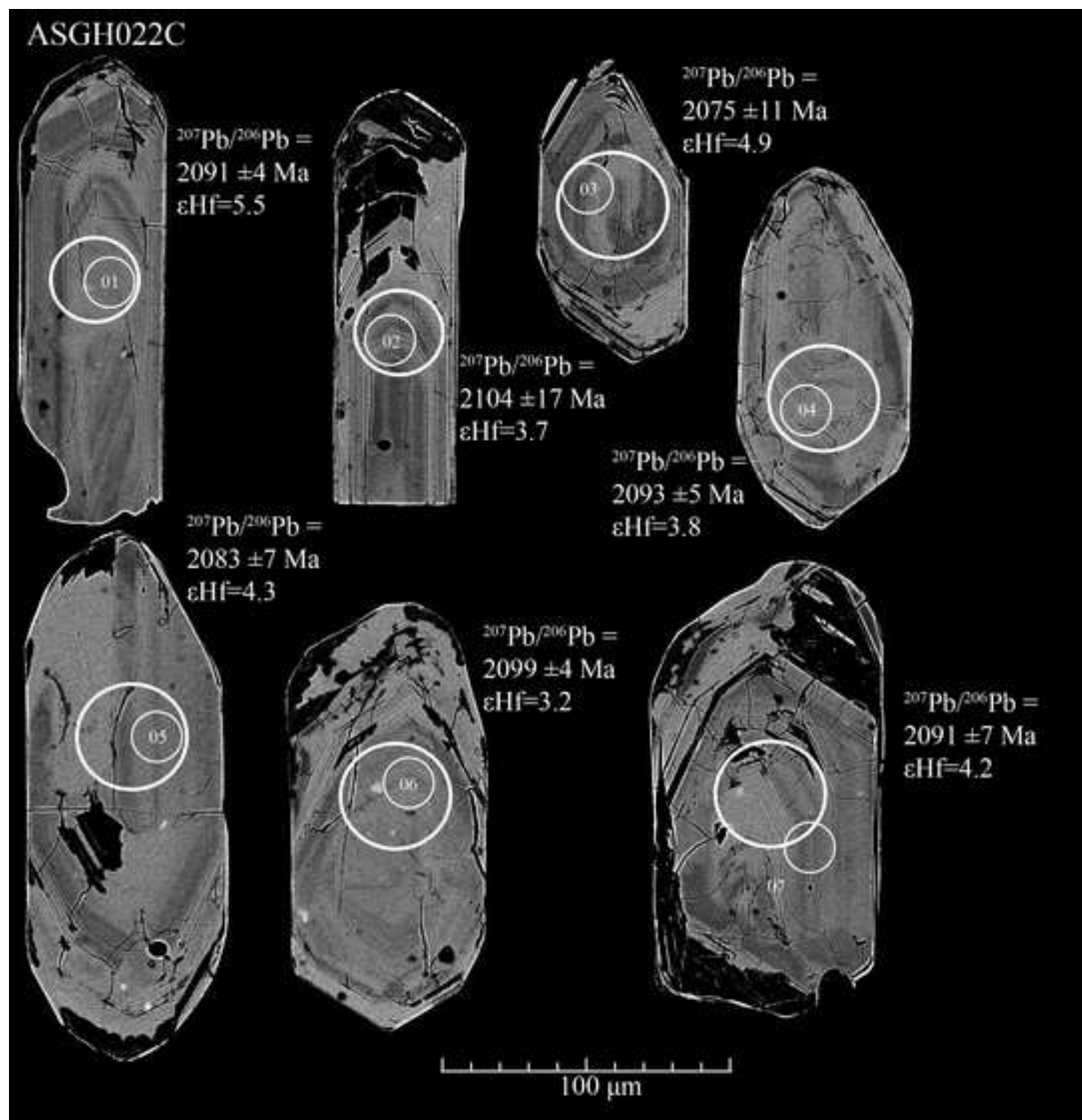


Figure 9





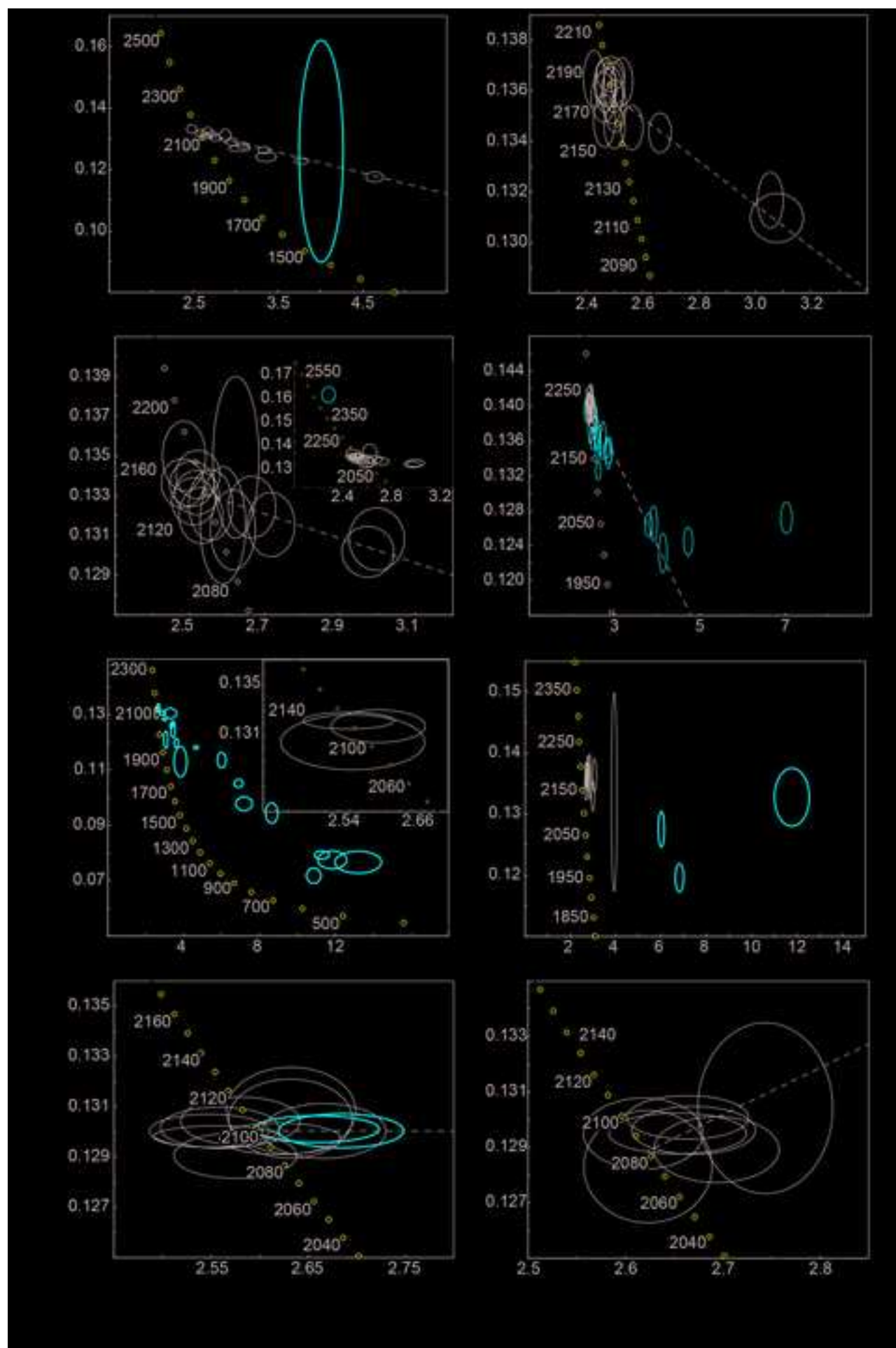


Figure 12

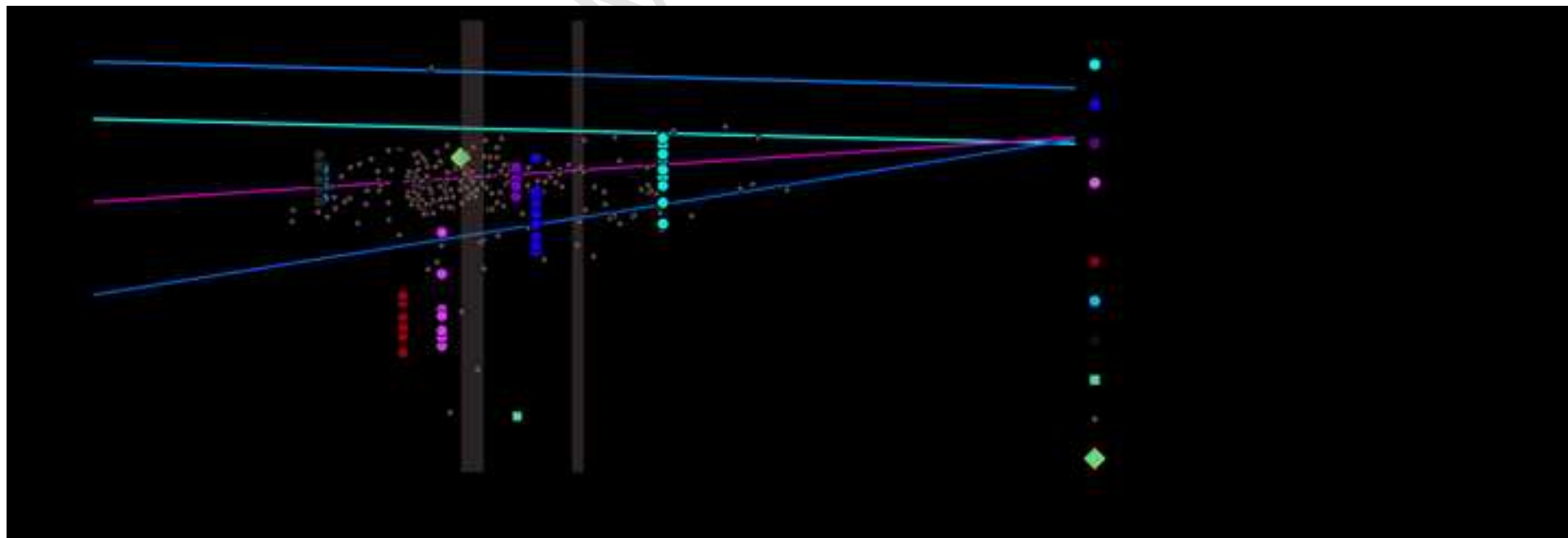


Figure 13

